Feedback inhibition by a descending GABAergic neuron regulates timing of escape behavior in *Drosophila* larvae

Jiayi Zhu[1,2], Jean-Christophe Boivin[1,2], Alastair Garner[1,2], Jing Ning[1], Yi Qing Zhao[1], Tomoko Ohyama[1,2,3*]

[1] Department of Biology, McGill University, Docteur Penfield Ave., Montreal, QC, H3A 1B1, Canada
[2] Integrated Program of Neuroscience, Pine Ave. W., McGill University, Montreal, QC, H3A 1A1, Canada
[3] Alan Edwards Center for Research on Pain, McGill University, University St., Montreal, QC, H3A 2B4, Canada

*Correspondence: tomoko.ohyama@mcgill.ca

Keywords: escape behavior, nociceptive circuit, descending neuron, GABA, *Drosophila*

Abstract

Escape behaviors help animals avoid harm from predators and other threats in the environment. Successful escape relies on integrating information from multiple stimulus modalities (of external or internal origin) to compute trajectories toward safe locations, choose between actions that satisfy competing motivations, and execute other strategies that ensure survival. To this end, escape behaviors must be adaptive. When a *Drosophila melanogaster* larva encounters a noxious stimulus, such as the focal pressure a parasitic wasp applies to the larval cuticle via its ovipositor, it initiates a characteristic escape response. The escape sequence consists of an initial abrupt bending, a corkscrew-like rolling, and finally rapid crawling. Previous work has shown that the detection of noxious stimuli primarily relies on class IV multi dendritic arborization neurons (Class IV neurons) located beneath the body wall, and more recent studies have identified several important components in the nociceptive neural circuitry involved in rolling. However, the neural mechanisms that underlie the rolling-escape sequence remain unclear. Here we present both functional and anatomical evidence suggesting that bilateral descending neurons within the

subesophageal zone of *D. melanogaster* larva play a crucial role in regulating the termination of rolling and subsequent transition to escape crawling. We demonstrate that these descending neurons (designated SeIN128) are inhibitory and receive inputs from a second-order interneuron upstream (Basin-2) and an ascending neuron downstream of Basin-2 (A00c). Together with optogenetic experiments showing that joint stimulation of SeIN128 neurons and Basin-2 influence the temporal dynamics of rolling, our findings collectively suggest that the ensemble of SeIN128, Basin-2, and A00c neurons forms a GABAergic feedback loop onto Basin-2, which inhibits rolling and thereby facilitates the shift to escape crawling.

Introduction

Virtually all organisms on earth face the threat of being maimed or killed by one or more predatory organisms. Not surprisingly, when organisms encounter threat-associated stimuli, they exhibit a wide variety of escape responses appropriate to their biological construction and the specific predators within their ecological niche (Burrell, 2017; Campagner et al., 2023; Chin & Tracey, 2017; Im & Galko, 2012; Peirs & Seal, 2016). Typically, these escape responses consist of a sequence of simple actions. The roundworm *C. elegans*, for example, in response to a touch to its head, exhibits rapid backward locomotion coupled with a suppression of head movements, followed by a deep ventral bend (omega turn) and a 180-degree reversal in the direction of locomotion. This sequence allows the roundworm to escape from nematophagal fungi that cohabitate with it in organic debris (Chalfie & Sulston, 1981; Chalfie et al., 1985).

When *Drosophila melanogaster* larvae encounter noxious stimuli, such as the stimulation that accompanies an attempt by a parasitic wasp to penetrate the larval cuticle with its ovipositor, they exhibit an escape response consisting of an initial abrupt bending, followed by corkscrew-like rolling, and finally, rapid crawling (Hwang et al., 2007; Ohyama et al., 2015; Onodera et al., 2017; Tracey et al., 2003). Previous work has shown that noxious stimuli are primarily detected by class IV dendritic arborization neurons (Class IV neurons) located beneath the body wall (Tracey et al., 2003). More recent studies have identified several important components in the downstream nociceptive neural circuitry, particularly those involved rolling (Burgos et al., 2018; Dason et al., 2020; Hu et al., 2017; Hu et al., 2020; Imambocus et al., 2022; Kaneko et al., 2017; Ohyama et al., 2015; Takagi et al., 2017; Yoshino et al., 2017). To date, however, the neural

mechanisms that underlie the rolling-escape sequence, notably, the transition from rolling to crawling, have remained unclear.

In this study, we provide both functional and anatomical evidence that, bilateral descending neurons in the subesophageal zone (SEZ) of *D. melanogaster* larva, which comprise part of a neural circuit underlying rolling, a characteristic nocifensive escape response, potentially regulates the termination of rolling and subsequent transition to escape crawling. We show that these descending neurons, which we designate as SeIN128, are identical to those denoted previously as SS04185 (Ohyama et al., 2015), are inhibitory neurons that receive inputs from Basin-2 (a second-order interneuron upstream) and A00c (an ascending neuron downstream of Basin-2), and provide GABAergic feedback onto Basin-2. Together with behavioral analyses of rolling during systematic optogenetic manipulation of SeIN128 and Basin-2 activity, our findings suggest that an ensemble of neurons—SeIN128, Basin-2, and A00c—forms an inhibitory feedback circuit that inhibits rolling, which in turn facilitates the shift to escape crawling.

SS04185 facilitates rolling termination and shortens the latency of crawling behavior in the escape responses

In a previous study, we showed that activation of all Basin neurons (Basin-1, -2, -3, and -4) induced rolling followed by fast crawling (Ohyama et al., 2015). Here, we first examined whether optogenetic activation of all four Basins expressing the red-shifted opsin CsChrimson (using Basin-1–Basin-4 Gal4, i.e., R72F11-Gal4) could elicit the same behavior. Upon activation of all Basins, we observed rolling mostly within the first 5 s, followed by crawling (Figure 1A and B). Crawling speed during the activation of all Basins following rolling was ~1.5 times that of the crawling speed at baseline (Figure 1B) (Ohyama et al., 2015).

To identify the neurons responsible for escape behavior (rolling and/or fast crawling), we conducted a behavioral screening of ~250 split Gal4 lines that were labeled in the central nervous system (CNS) when co-activated with all Basins. With respect to rolling, we found that activation of the split-Gal4 line, SS04185 (i.e., w^{1118}; $R54B01\text{-}Gal4^{AD}$; $R46E07\text{-}Gal4^{DBD}$), significantly reduced the probability of rolling when compared to activating only the Basins (Figure 1A–C).

The likelihood of rolling upon joint activation of SS04185 neurons and Basins might decrease because activation of SS04185 neurons trigger other actions, such as crawling, head casting,

hunching, or stopping, and not because they solely inhibit rolling evoked by Basins. To investigate this possibility, we examined the effect of SS04185 activation in isolation and found that this did not induce any extra actions such as turning, hunching, or stopping (Figure 1–figure supplement 1A-D). These data suggest that joint activation of Basins and SS04185 neurons reduces rolling because SS4185 activation inhibits the Basin circuit.

Next, we explored how the quality of rolling changed during joint activation of SS04185 and Basin neurons. First, we examined the amount of time animals spent rolling during Basin activation. The average time spent rolling (percentage of the 30-s stimulation period) was 23.9% (7.2 s out of 30 s) following activation of Basins alone, whereas it was only 5.9% following joint activation of Basins with SS04185 (1.8 s out of 30 s) (Figure 1–figure supplement 1E). Additionally, the duration of each rolling bout was significantly shorter when SS04185 neurons were co-activated with Basins (Mann-Whitney U test, $p < 0.001$; Figure 1D).

The duration of a rolling bouts could decrease because of changes in the latency to initiate rolling, latency to terminate rolling, or both. To investigate how SS04185 activation affects these temporal parameters of rolling, we analyzed the latencies for the initiation and termination of the first rolling bout. Compared to activating Basins alone, co-activating the Basins and SS04185-expressing neurons only marginally increased latency to onset of the first rolling bout (Figure 1E), whereas it markedly reduced the latency for the termination of rolling (Mann-Whitney U test, $p < 0.001$; Figure 1F). These data strongly suggest that SS04185-expressing neurons are involved in terminating rolling.

If the rolling module inhibits crawling, then premature termination of rolling might allow crawling to commence sooner than normal. Joint activation of SS04185 and Basins resulted in the initiation of the first crawling bout occurring earlier than when only Basins were activated (Mann Whitney U test, $p < 0.001$; Figure 1G, Figure 1–figure supplement 1F). The time from the end of rolling to the start of crawling remained similar between the groups in which the Basins were activated alone and in which the Basins and SS04185 were co-activated (Figure 1–figure supplement 1G). This is consistent with the higher probability of crawling during activation of SS04185 and Basin neurons (Figure 1–figure supplement 1H). Lastly, activation of SS04185 neurons in conjunction with Basins did not change the crawling speed compared to activation of Basins alone (Figure 1–figure supplement 1I). These results collectively indicate that SS04185 activation terminates rolling and facilitates the shift to fast crawling.

A pair of descending neurons in SS04185 contributes to termination of rolling

To identify the neurons that express SS04185 upon CsChrimson activation, we examined the localization of SS04185-labeled neurons. We found that SS04185 split-Gal4 strongly labeled a pair of descending neurons located within the subesophageal zone (SEZ) and mushroom body (MB) neurons within the brain (Figure 2A). To pinpoint which of these neurons are involved in reducing the probability of rolling (Figure 1A-C), we varied the level of SS04185 expression among the pair of SS04185-expressing descending neurons (SS04185-DN) and the SS04185-expressing MB (SS04185-MB) neurons (jointly with the Basins as in Figure 1). These manipulations allowed us to assess the resultant behavioral outcomes.

If SS04185-MB neurons are involved in the modulation of rolling, then reducing SS04185-MB expression should reduce the extent to which activation of both SS04185-DN neurons and SS04185-MB neurons decreases the probability of rolling. To test this conjecture, we expressed Killer Zipper ($KZip^{+}$), which interferes with the binding of $Gal4^{AD}$ and $Gal4^{DBD}$ in SS04185-MB neurons with MB LexA line (R13F02-LexA), consequently leading to a significant reduction in CsChrimson expression in SS4185-MB neurons (Figure 2B, Figure 2–figure supplement 1A) (Dolan et al., 2017; Vogt et al., 2016). When compared to $KZip^{+}$ controls, which do not express SS04185 (Figure 2C, black bars), however, activation of SS04185 neurons with reduced SS04185-MB expression (Figure 2C, red bars on the right; Figure 2–figure supplement 1B) still reduced rolling probability (as well as the total duration of rolling [Figure 2–figure supplement 1C]) to a level no different from that of $KZip^{-}$ controls expressing SS04185 fully in both SS04185-MB and SS04185-DN neurons (Figure 2C, dark red bars in the middle). Additionally, co-activation of MB Gal4 lines (MB247-Gal4) with Basins (without activation of SS04185-DN neurons) did not reduce the probability of rolling (Figure 2–figure supplement 1D-E) (Pauls et al., 2010). These data indicate that SS04185-DN neurons inhibit rolling.

To further test the role of SS04185-DN neurons, we investigated whether these neurons were involved in reducing the duration of each rolling bout (Figure 1A, D, F). However, knockdown of SS04185-MB neurons did not increase the duration of rolling bouts (Figure 2D). Furthermore, the earlier onset of crawling triggered by the activation of SS04185 neurons remained the same with knockdown of SS04185-MB neurons (Figure 2E). Collectively, these results strongly

suggest that the behavioral effects on both rolling and crawling, as illustrated in figure 1, are primarily mediated by SS04185-DN neurons.

To further ascertain the role of SS04185-DN neurons in the regulation of rolling, we employed the heat shock FlpOut mosaic expression approach. This technique allowed for controlled and sporadic expression of CsChrimson in SS04185 neurons thorough random induction of Flippase by manipulating the timing and duration of heat shock (Golic and Lindquist, 1989; Nern et al., 2015). We compared larvae subjected to activation of both SS04185-MB and SS04185-DN neurons (red, Figure 2–figure supplement 1F) with those subjected only to activation of SS04185-MB neurons (black, Figure 2–figure supplement 1G), to assess the degree to which the former showed behavioral effects. Remarkably, activation of both SS04185-MB and SS04185-DN neurons resulted in a reduction in both the probability and duration of rolling when compared to activation of SS04185-MB neurons alone (Figure 2F and G, Figure 2–figure supplement 1H-I). Furthermore, activation of both SS04185-MB and SS04185-DN neurons reduced the latency to the end of the first rolling bout and the initiation of the first crawling bout (Figure 2H, Figure 2–figure supplement 1J). These findings provide compelling evidence that SS04185-DN neurons, but not SS04185-MB neurons, play an important role in the termination of rolling.

Descending neurons identified by SS04185 correspond to SeIN128 neurons

In a previous EM study, we identified a set of neurons designated as SeIN128, whose cell bodies in the SEZ send axonal projections throughout the thoracic and abdominal segments (Figure 3A) (Ohyama et al., 2015). Our immunostaining data also showed that the cell bodies of SS04185-DN neurons are located in the SEZ, with axons bilaterally innervating the medial regions of the VNC from the thoracic to abdominal segments A8/9 (Figure 2A), suggesting that SS04185-DN and SeIN128 neurons are one and the same.

To verify this possibility, we examined the detailed anatomy of SS04185-DN neurons by immunostaining them with several markers and compared our immunostaining images with the corresponding images obtained via EM reconstruction of the entire CNS of a 1st instar *Drosophila* larva (Ohyama et al., 2015; Winding et al., 2023). We confirmed that the projections of SeIN128 neurons are distributed within the ventromedial neural tract (one of the six major neural tracts) in *Drosophila* larvae (Figure 3A, B, and C) in EM reconstruction data. We also

confirmed that the cell bodies of SS04185-DN neurons were again located in the SEZ region, where the most anterior of the three neuropils in the thoracic region was marked by N-cadherin (Figure 3D). Viewed from the side (i.e., in the longitudinal or sagittal plane), both the cell bodies and axonal arbor were located ventrally (Figure 3D, far right). Immunostaining with Fasciclin2 (Fas2), which labels various neural tracts in the VNC (Grenningloh et al., 1991; Santos et al., 2007), showed colocalization of the axonal projections of SS04185-DN neurons and the Fas2-labeled ventromedial tract (Figure 3C and E). The similarity of the locations of their cell bodies and the distributions of their axonal processes suggests the identity of the SS04185-DN and SeIN128 neurons.

A previous EM study showed that SeIN128 neurons were located downstream of Basin neurons (Ohyama et al., 2015). To further confirm the identity of SS04185-DN and SeIN128 neurons, we compared the distributions of the axonal projections of SS04185-DN neurons in relation to those of several key neurons within the rolling circuit: the Basins, A00c neurons (a group of ascending neurons downstream of the Basins, and which facilitate rolling), and mdIV neurons (nociceptive sensory neurons upstream of the Basins). Immunostaining revealed that Basin projections colocalize with those of SS04185-DN neurons in both the horizontal and transverse planes (Figure 3F, top and lower panels, respectively), with the horizontal view showing that SS04185-DN projections are distributed slightly medial to those of Basins within the ventromedial tract (Figure 3F, top panels), which resembles their colocalization pattern reported in EM (Figure 3B, C and G). Similarly, we compared the distributions of SS04185-DN projections with those of A00c or mdIV projections. We found that the projections of A00c colocalize with those of SS04185-DN in a similar fashion along the rostrocaudal axis within the ventromedial tract (Figure 3H and I), with A00c projections distributed more medially than SS04185-DN projections, consistent with the distribution patterns of SeIN128 projections and A00c projections in the EM reconstruction dataset (Figure 3B, H and I). In contrast, the distributions of mdIV projections did not colocalize with those of SS04185-DN projections, as the mdIV projections were displaced more laterally relative to the SS04185-DN projections in the horizontal and transverse planes (Figure 3J, top and lower panels, respectively), consistent with the distribution patterns of SeIN128 and mdIV projections in the EM reconstruction dataset (Figure 3K). In the transverse plane, the projections of SS04185-DN neurons were also

distributed dorsomedial to those of mdIV (Figure 3J, lower panel), consistent with the corresponding distribution patterns in the EM reconstruction dataset (Figure 3B, C and K).

We conclude that the morphological findings for SS04185-DN neurons, together with data on the distribution of their axonal projections in relation to that of Basin, A00c, and mdIV neurons, strongly suggest the identity of SS04185-DN and SeIN128 neurons.

Connectome and functional connectivity analyses: SeIN128 neurons receive inputs from Basin-2 and A00c

A previous study that reconstructed larval neurons involved in the rolling circuit showed that Basin-2 and A00c neurons (in the VNC) make excitatory synaptic contacts onto SeIN128 neurons (in the CNS), which in turn make reciprocal inhibitory synaptic contacts onto Basin-2 and A00c neurons (Figure 4A, Figure 4–figure supplement 1A) (Ohyama et al., 2015). These data suggest that SeIN128 neurons are directly activated by Basin-2 and A00C (which also receives inputs from Basin-1, Basin-2, and Basin-4).

To assess the functional significance of these synaptic connections between SeIN128 neurons and Basins or A00c, we activated either Basins or A00c neurons and examined the resultant GCaMP signaling in SeIN128 neurons. Specifically, after expressing CsChrimson in Basins and A00c neurons and GCaMP in SeIN128 neurons, we used a two-photon microscope (920-nm laser) and monitored GCaMP signaling in SeIN128 neurons during illumination of a specimen with a 620-nm LED for 1 s (0.04–1.4 $\mu W/mm^2$), which activated either Basins or A00c neurons. GCaMP signals in SeIN128 neurons increased in an intensity-dependent manner when either Basins and A00c were activated (Figure 4B and C). Peak activity occurred at around 3 s after the onset of LED stimulation, which was similar to the results when Basins or A00c neurons were stimulated (Figure 4B and C). Finally, both Basin and A00c stimulation resulted in linear dose-dependent increases in SeIN128 firing (Figure 4–figure supplement 1B). These results are consistent with the notion that SeIN128 neurons are downstream of Basins or A00c neurons.

To compare the neural responses between Basins and SeIN128 or A00c neurons, we recorded neural activity in A00c neurons with GCaMP while stimulating Basin neurons in the same experimental setting. Although A00c neurons displayed a similar dose-dependent increase in peak axonal firing as the intensity of optogenetic stimulation of Basin neurons increased, unlike SeIN128 neurons they showed no delay in peak firing activity (Figure 4D and E, Figure 4—

figure supplement 1B), suggesting that A00c and SeIN128 neurons function differently in the rolling circuit.

We then investigated the anatomical locations of the synaptic outputs and inputs of SeIN128 neurons, and found that, whereas their outgoing projections primarily make synaptic contacts along the anterior-posterior nerve axis, the inputs coming from other neurons are mainly located in the SEZ (Figure 3A). These data suggest that the main synaptic inputs onto SeIN128 neurons in the SEZ mediate the slow responses upon activation of Basins or A00c neurons. On the other hand, SeIN128 neurons make axo-axonal contacts onto Basin-2 neurons (Figure 4–figure supplement 2A-G): that is, their axons make synaptic contacts with the dorsal and medial processes of Basin-2, which correspond to their axonal compartments (Figure 4–figure supplement 2E-G). These axo-axonal connections could modulate the output of Basin neurons without affecting the activity at their cell bodies induced by other neural inputs.

SeIN128 neurons are GABAergic and inhibitory

The results thus far indicate that activation of SeIN128 neurons inhibits rolling (Figure 1A–C) and that SeIN128 neurons provide inputs onto Basin-2 and A00c (Figure 4A). These findings suggest that SeIN128 neurons might be inhibitory. To test this possibility, we performed immunostaining experiments and found that SeIN128 neurons colocalized with glutamic acid decarboxylase (Gad)-positive neurons but not with acetylcholine- or glutamate-positive neurons, suggesting that SeIN128 neurons are GABAergic inhibitory neurons (Figure 5A, Figure 5–figure supplement 1A, and B).

We reasoned that if GABA in SeIN128 neurons is necessary for inhibiting rolling, then selectively knocking down GABA secretion in SeIN128 neurons should enhance rolling. When we expressed RNAi *HMS02355* in SeIN128 neurons to knock down vesicular GABA transporter (VGAT) expression and suppress the release of GABA, the population-level rolling probability increased from 23.6% to 45.2% (Figure 5B and C) (Kallman et al., 2015; Zhao et al., 2019). Furthermore, the duration of each bout of rolling increased from 0.8 s to 1.4 s (Figure 5D). These data support the idea that SeIN128 neurons inhibit rolling via GABAergic transmission.

Inhibition of SeIN128 increases probability and duration of rolling

To further test whether the release of GABA upon activating SeIN128 neurons is necessary for inhibiting rolling, we expressed tetanus toxin (TNT) in SeIN128 neurons to block synaptic transmission. Silencing SeIN128 neurons via TNT while triggering rolling by optogenetically activating Basin neurons via *R72F11-LexA>LexAop-CsChrimson* significantly increased the probability of rolling compared to controls (Figure 6A and B). Silencing SeIN128 neurons via TNT extended the duration of each rolling bout, as well as the total rolling duration, in each larva (Figure 6C and D). We also examined the rolling-escape crawling sequence upon silencing SeIN128 neurons, and found that the time to offset of rolling and the time onset of crawling were both delayed relative to controls (Figure 6E and F).

Given that TNT is expressed constitutively during development, long-term compensatory changes in the nervous system could have contributed to alterations in the parameters of rolling and crawling. To test whether similar results could be replicated with the use of a temporally specific intervention, we expressed *shibire*^{ts1} (*shi*^{ts1}) in SeIN128 neurons to block synaptic transmission at temperatures above 30°C (van de Goor et al., 1995; Kitamoto, 2001). Silencing SeIN128 neurons via *shibire*^{ts1} increased the probability of rolling from 60.4% to 79.7% (Figure 6–figure supplement 1A and B). The total duration of rolling per animal during stimulation increased from 10 to 12 s (Figure 6–figure supplement 1C). Although the duration of each rolling bout and the time to onset of the first rolling bout did not differ from those of controls (Figure 6–figure supplement 1D and E), the time to offset of the first rolling bout and time to onset of the first crawling bout were both delayed relative to those of controls ($p = 0.013$ for Figure 6–figure supplement 1F; $p = 0.11$ for Figure 6–figure supplement 1G). Together with the results showing that activation of SeIN128 neurons inhibits rolling, these findings suggest that the activity of SeIN128 neurons is important in controlling the duration of rolling and the shift to crawling.

Basins receive GABAergic inputs that inhibit rolling

Given that Basins receive axo-axonal inputs from SeIN128 neurons and GABA signaling in SeIN128 neurons inhibits rolling, we next used RNA interference (RNAi) to test whether Basins receive GABAergic signals from SeIN128. We hypothesized that knockdown of GABA receptors in Basin neurons would increase the probability and duration of rolling at the population level. To knock down ionotropic GABA-A receptors (GABA-A-R) and G-protein-coupled GABA-B receptors (GABA-B-R1 and GABA-B-R2), we tested Basin neurons with GABA-A-R, GABA-

B-R1, and GABA-B-R2 RNAi lines (i.e., *HMC03643* for GABA-A-R, *HMC03388* for GABA-B-R1[1], *JF02989* for GABA-B-R1[2] and *HMC02975* for GABA-B-R2, respectively). For all RNAi lines, the rolling probability at the population level increased from 80% to 90% or even higher (Figure 7A), while the total rolling duration at the individual level increased for each larva throughout the stimulation window (Figure 7–figure supplement 1A). All GABA receptor knockdown groups showed significant increases in rolling duration across multiple bouts (Figure 7B); all groups except for GABA-B-R1[1] showed a reduced time to onset of the first rolling bout (Figure 7–figure supplement 1B); and only the GABA-B-R2 and GABA-A-R groups showed a delayed offset of the first rolling bout (Figure 7–figure supplement 1C). None of the groups differed from controls in the time to onset of the first crawling bout (Figure 7–figure supplement 1D). The greatest increase in the probability and duration of rolling was seen during knockdown of ionotropic GABA-A-R (*Rdl*), suggesting that Rdl contributes most to the inhibition of Basin neurons (Figure 7A and B).

To investigate whether SeIN128 neurons actually inhibit Basins, we recorded the activity of all Basins during activation of SeIN128 neurons. We compared GCaMP signaling in the Basins when they were co-activated with SeIN128 neurons (experimental treatment) or when they were activated alone (control treatment), with the intensity of optogenetic stimulation varied from 0.04 to 1.4 $\mu W/mm^2$. We found that Basins in the experimental group showed reductions in GCaMP signaling by 8% to 33% compared to those in the control group (Figure 7C, Figure 7–figure supplement 1E and F). The reductions were observed at all stimulation intensities when contrasting peak GCaMP responses, and statistically significant at intensities of 0.3 and 0.5 $\mu W/mm^2$ (Figure 7C, Figure 7–figure supplement 1E and F). Collectively, these data support the idea that SeIN128 neurons directly inhibit the activity of Basins via GABA.

Effects of SeIN128 activation on rolling elicited by activating individual Basins

In the studies above, we measured the activity of all Basins while manipulating the activity of SeIN128 neurons. Connectome and behavioral analyses indicate, however, that of the four types of Basins, only Basin-2 and Basin-4 receive nociceptive input from mdIV and trigger rolling (Ohyama et al., 2015). Moreover, as noted above, an examination of the larval connectome (Ohyama et al., 2015; Winding et al., 2023) revealed that Basin-2 both receives axo-axonal inputs from SeIN128 neurons and sends excitatory projections to the same SeIN128 neurons,

whereas a similar examination revealed that Basin-4 neither receives inputs from, nor sends any outputs to, SeiN128 neurons. Therefore, we hypothesized that activation of SeIN128 neurons would inhibit rolling elicited by Basin-2 activation and modify the temporal parameters of rolling, but not affect rolling elicited by Basin-4 activation.

We first examined the pattern of rolling evoked by optogenetically activating Basin-2. Basin-2 activation induced multiple bouts of rolling throughout the stimulation window (Figure8–figure supplement 1A). Furthermore, the rolling elicited by Basin-2 activation tended to be sustained (Figure8–figure supplement 1A). Next, to determine how SeIN128 activation affects the pattern of rolling elicited by Basin-2 activation, we optogenetically activated SeIN128 neurons and Basin-2 simultaneously. As expected, compared to the probability of rolling in control animals in which only Basin-2 was activated, the probability of rolling in experimental animals in which Basin-2 and SeIN128 neurons were simultaneously activated was significantly lower (66.7% vs 24.4%; Figure 8A, Figure 8–figure supplement 1D). We also examined other parameters of rolling, including the time from the start (onset) of stimulation to the onset of the first rolling bout, termination (offset) of the first rolling bout, and onset of the first crawling bout, as well as the duration of the rolling bout (i.e., the time from its onset to its offset). Consistent with the hypothesis that SeIN128 activation inhibits Basin-2 activity, the duration of the rolling bout significantly decreased (Figure 8B, Mann-Whitney test, $p = 0.0034$, *Cohen's d* = 0.351) and the time to onset of the first rolling bout significantly increased in experimental animals compared to controls (Figure 8–figure supplement 1E; Mann-Whitney test, $p < 0.001$). In addition, as expected, the time to offset of the first rolling bout (Figure 8C; Mann-Whitney test, $p = 0.0047$, *Cohen's d* = 0.607) and time to onset of the first crawling bout (Figure 8D; Mann-Whitney test, $p = 0.0074$, *Cohen's d* = 0.548) both significantly decreased in experimental animals compared to controls. Collectively, these findings suggest that Basin-2 neurons play a major role in mediating the effects of SeIN128 activation on rolling induced by optogenetic activation of all Basin neurons.

To ascertain our expectation that SeIN128 activation would have little if any effect on the pattern of rolling elicited by Basin-4 activation, given the absence of any identifiable synaptic contacts between Basin-4 neurons and SeIN128 neurons based on available information on the larval connectome, we also carried out the same analyses as those described above for rolling elicited by Basin-2 activation. We examined the pattern of rolling evoked by optogenetically activating

Basin-4, and found that this manipulation induced rolling mostly within the first 5 s of stimulation (Figure 8–figure supplement 1B and F). Consequently, at the population level, rolling elicited by Basin-4 activation was transient compared to the rolling elicited by Basin-2 activation (compare Figure 8–figure supplement 1A vs 1B) (Figure 8–figure supplement 1C).

We then assessed whether SeIN128 activation would affect rolling elicited by Basin-4 activation. Surprisingly, compared to control animals, the probability of rolling in experimental animals was significantly lower (66.7% vs 26.8%; Figure 8E), much as was the case for rolling elicited by Basin-2 activation. We also examined the other rolling parameters, and found that the duration of the rolling bouts (Figure 8F; Mann-Whitney test, $p = 0.032$, *Cohen's d = 0.248*), time to offset of the first rolling bout (Figure 8G; Mann-Whitney test, $p < 0.0047$, *Cohen's d = 0.427*), and time to onset of the first crawling bout (Figure 8H; Mann-Whitney test, $p < 0.001$, *Cohen's d = 1.039*) all significantly decreased in experimental animals compared to controls, although the effect sizes were smaller compared to those observed for rolling elicited by Basin-2 activation. The time to onset of the first rolling bout, however, did not significantly differ between experimental animals and controls (Figure 8–figure supplement 1G). These findings suggest the possibility that sites further downstream of Basin-4 neurons may be involved in inhibitory processes that affect rolling elicited by Basin-4 activation.

Discussion

In this study, we provide both anatomical and functional evidence that, bilateral descending neurons in the brain of *D. melanogaster* larva, which comprise part of a neural circuit underlying a characteristic rolling response that larvae exhibit when evading parasitization by wasps, potentially regulates the termination of rolling and the subsequent transition to escape crawling. We showed that these descending neurons, which we designated as SeIN128, were identical to those previously identified as a component of the nociceptive circuit; were inhibitory neurons that receive excitatory inputs from Basin-2, a second-order interneuron upstream, and A00c, an ascending neuron downstream of Basin-2; and provided GABAergic feedback onto Basin-2, presumably via the axo-axonal synaptic contacts made by the axon terminal endings of SeIN128 neurons onto the axons of Basin-2. Optogenetic activation studies further showed that joint stimulation of SeIN128 and Basin-2 neurons systematically altered the temporal dynamics of rolling and subsequent escape crawling. Collectively, the evidence suggests that the ensemble of

SeIN128, Basin-2, and A00c neurons constitutes a novel inhibitory feedback circuit that provides reduces Basin-2 activity, which in turn, here influence the activity of a key interneuron of the rolling circuit via a novel inhibitory mechanism.

Feedback inhibition in a nociceptive circuit

Feedback inhibition occurs when an excitatory neuron sends projections to an inhibitory neuron, which in turn sends projections back onto the same excitatory neuron, often at its presynaptic terminals (Isaacson & Scanziani, 2011; Kapfer et al., 2007; Ray et al., 2020; Stokes & Isaacson, 2010; Yoshimura & Callaway, 2005). The hallmark of feedback inhibition lies in its ability to modulate the duration and magnitude of incoming excitatory signals, thereby fine-tuning neural responses and maintaining homeostasis (Kapfer et al., 2007; Papadopoulou et al., 2011; Stokes & Isaacson, 2010; Yoshimura & Callaway, 2005). Compared to the fast temporal dynamics of feedforward inhibition, in which an inhibitory neuron directly inhibits an excitatory neuron downstream of it, the temporal dynamics of feedback inhibition are slower, primarily due to the added synaptic delays (two or more) following activation of an excitatory neuron (Papadopoulou et al., 2011; Ray et al., 2020; Stokes & Isaacson, 2010). The slow temporal dynamics serve to inhibit the sustained neural activity and magnitude of incoming excitatory signals (Papadopoulou et al., 2011; Ray et al., 2020; Stokes & Isaacson, 2010).

In this study, we showed that SeIN128 neurons are descending neurons whose main inputs arrive in the brain and SEZ regions, and whose outputs target the VNC. We also found that SeIN128 neurons receive excitatory inputs from Basin-2 as well as its downstream neuron A00c, and in turn send inhibitory projections back to these neurons in the VNC, potentially establishing a feedback inhibition motif that modulates the nociceptive rolling circuit. The interplay we observed among SeIN128 neurons, Basin-2, and A00c are consistent with this view. Our findings revealed that activation of SeIN128 neurons has a suppressive effect on Basin-2 activity and, notably, on the duration of rolling. These observations support the idea that feedback inhibition is critical in regulating the temporal aspects of nociceptive responses.

Inhibition of Basin-2 by SeIN128 neurons is mediated by axo-axonal synapses

Neurons form a wide variety of neural networks that perform various computations in the brain. Typically, a neuron receives inputs via axo-dendritic synapses (i.e., contacts made by the axon terminals of an upstream neuron with its dendrites), which play a role in the spatial and temporal computations that lead to the firing of action potentials. Less commonly, the axon terminals of an

upstream neuron may contact the soma (i.e., via axo-somatic synapses) or axon (i.e., via axo-axonal synapses) of a downstream neuron (Palay, 1956; Pinault et al., 1997; Zheng et al., 2018). Axo-axonal synapses have a subtle effect on neurotransmission at the network level because the activity in presynaptic neurons does not alter the membrane potential (Cattaert & El Manira, 1999; Guo & Hu, 2014; McGann, 2013). Axo-axonal synapses mainly affect the release probability of neurotransmitter vesicles in response to an action potential triggered in the postsynaptic neuron (McGann, 2013; Oleson et al., 2012).

Recent studies suggest that the activity of axo-axonal synapses can prevent the transmission of action potentials. For example, it has been reported that, neurotransmission mediated by type-B muscarinic receptors at lateral axo-axonal connections between *Drosophila* Kenyon Cells is critical for stimulus specificity learning in drosophila (Manoim et al., 2022); inhibitory axo-axonal connections between Chandelier cells and CA1 pyramidal cells are important for activity-dependent plasticity (Pan-Vazquez et al., 2020; Schneider-Mizell et al., 2021); and GABAergic axo-axonal interneurons in the amygdala are crucial for generating action potentials in the principal output cells (Veres et al., 2023). Furthermore, EM connectome analyses of the entire larval brain reveal that ~70% of all synapses in drosophila larvae are axo-dendritic whereas ~30% are axo-axonal, suggesting that the latter may have considerable influence over network function (Winding et al., 2023).

In this study, we found a feedback connection between SeIN128 and Basin-2 mediated by axon-axonal synapses (Figure4 – supplementary 2E-G). The slow increase of SeIN128 activity in response to Basin-2 or A00c activation could potentially occur because of these axo-axonal connections. This delayed activity may play an important role in the feedback inhibition of Basin-2 activity, and in turn, the termination of rolling.

Roles of Basin-2 and Basin-4 in escape behavior

Previous studies have shown that, Basin-2 and Basin-4 receive both chordotonal sensory and nociceptive sensory inputs, and in addition, play a critical role in escape behavior (Ohyama et al., 2015). Here we investigated the differences between rolling induced by activation of Basin-2 or Basin-4. We found that activation of Basin-2 induced rolling that was sustained. Furthermore, activation of SeIN128 neurons reduced the duration of rolling induced by joint activation of Basin-2, which resulted in a delay in the onset of rolling and an earlier termination of rolling. These data indicate that activation of Basin-2 serves to maintain rolling. Connectome data

indicate that SeIN128 neurons provide inhibitory input onto Basin-2, which is consistent with the finding that SeIN128 activation reduces the duration of rolling.

On the other hand, activation of Basin-4 induced rolling that was transient, which was then followed by rapid crawling. Furthermore, activation of SeIN128 neurons reduced the probability of rolling but did not affect the duration of rolling (Figure 8F). This suggests that activation of Basin-4 is important for the induction of rolling, but not its maintenance. The behavioral effects of coactivating SeIN128 and Basin-4, together with connectome data indicating the lack of any connections between SeIN128 neurons and Basin-4, suggest that these descending neurons target neurons downstream of Basin-4 neurons.

Other inputs onto SeIN128 neurons modify escape behavior

The dendritic regions of SeIN128 neurons are located in the SEZ and brain, suggesting that SeIN128 neurons receive other inputs from SEZ and brain neurons. In this study, we did not examine these inputs. Connectome data indicate that MB output neurons project onto SeIN128 neurons (Ohyama et al., 2015). Given the well-established role of MB neurons in learning, this finding suggests that SeIN128 neurons could play a role in experience-dependent modulation of rolling. Two recent studies have shown that descending neurons inhibit nociceptive neurons (Nakamizo-Dojo et al., 2023; Oikawa et al., 2023). Specifically, one study showed that insulin signaling modulates escape behavior by activating GABAergic descending neurons that inhibit nociceptive sensory neurons (Nakamizo-Dojo et al., 2023), whereas the other demonstrated an inhibitory mechanism mediated by the neuropeptide Drosulfakinin, a homologue of cholecystokinin in mammals (Oikawa et al., 2023). Whether SeIN128 neurons are also influenced by insulin signaling or Drusulfakinin, however, remains to be seen.

In summary, our study delineates a neuronal ensemble consisting of a set of descending inhibitory neurons, a first-order interneuron (Basin-2), and an ascending neuron (A00c) in fruit fly larvae, which functions as an inhibitory feedback circuit that regulates the probability and duration of rolling, and thereby facilitates the transition from rolling to crawling. This work represents another example of how detailed analyses of connectomes and functional analyses of neural and behavioral activity can identify mechanistic explanations of behavioral phenomena at the level of neural circuits—in this case, how neuronal ensembles generate behavioral sequences.

Materials and Methods:

Key resources table

Reagent or resource	Source or reference	Identifiers
Antibodies		
Mouse anti-Brp monoclonal antibody, clone nc82	Developmental Studies Hybridoma Bank	Cat# nc82, RRID:AB_2314866
Mouse 1D4 anti-fasciclin II antibody	Developmental Studies Hybridoma Bank	Cat# 1D4 anti-Fasciclin II, RRID:AB_528235
Rat anti-cadherin, DN- (extracellular domain) antibody	Developmental Studies Hybridoma Bank	Cat# DN-Ex #8, RRID:AB_528121
Chicken anti-GFP antibody	Abcam	Cat# ab13970, RRID:AB_300798
Rabbit anti-GFP polyclonal antibody, unconjugated	Thermo Fisher Scientific	Cat# A-6455, RRID:AB_221570
Rabbit anti-DsRed polyclonal antibody	Takara Bio	Cat# 632496, RRID:AB_10013483
Mouse anti-Drosophila choline acetyltransferase monoclonal antibody, unconjugated	Developmental Studies Hybridoma Bank	Cat# chat4b1, RRID:AB_528122
Rabbit anti-GABA	Millipore Sigma	Cat # A2052
Rabbit anti-GLUT1	Gift from Aberbe lab	
Goat anti-chicken IgY (H+L) secondary antibody, Alexa Fluor™ 488	Thermo Fisher Scientific	Cat# A-11039, RRID:AB_2534096
Goat anti-rabbit IgG (H+L) highly cross-adsorbed secondary antibody, Alexa Fluor™ 488	Thermo Fisher Scientific	Cat# A-11034, RRID:AB_ 2576217
Goat anti-rabbit IgG (H+L) cross-adsorbed secondary antibody, Alexa Fluor™ 568	Thermo Fisher Scientific	Cat# A-11011, RRID:AB_143157
Goat anti-mouse IgG (H+L) cross-adsorbed secondary antibody, Alexa Fluor™ 568	Thermo Fisher Scientific	Cat# A-11004, RRID:AB_2534072
Goat anti-rat IgG (H+L) Alexa Fluor™ 568	Thermo Fisher Scientific	Cat# A-11077, RRID:AB_2534121
Chemicals		
PBS, Phosphate Buffered Saline, 10x solution	Fisher Scientific	Cat# BP399-1
Triton X-100	Millipore Sigma	Cat# X100-100ML
Paraformaldehyde 20% aqueous solution	Electron Microscopy Sciences	Cat# 15713
Normal goat serum	Gibco	PCN5000
VECTASHIELD antifade mounting medium	Vector Laboratories	Cat# H-1000-10
Drosophila Agar	Diamed	Cat# GEN66-103
All Trans Retinal	Toronto Research Chemicals Inc.	Cat# R24000
Poly-L-lysine	Sigma-Aldrich	Cat# P1524
Fly strains		
R72F11-Gal4 (attp2)	Bloomington Drosophila Stock Center	RRID: BDRC_39786
R71A10-Gal4 (attp2)	Bloomington Drosophila Stock Center	RRID: BDRC_39562
w; R54B01-Gal4^{AD};R46E07-Gal4^{DBD} (SS04185)	Gift from Zlatic lab	N/A
w; R72F11-Gal4^{AD};R38H09-Gal4^{DBD} (SS00739)	Gift from Zlatic lab	N/A
w; R72F11-Gal4^{AD};R57F07-Gal4^{DBD} (SS00740)	Gift from Zlatic lab	N/A
MB247-Gal4, mef2-Gal4	Bloomington Drosophila	RRID:

	Stock Center	BDRC_50742
R13F02-LexA (attp40)	Bloomington Drosophila Stock Center	RRID: BDRC_52460
R72F11-LexA (attp40)	Bloomington Drosophila Stock Center	RRID: BDRC_94661
R71A10-LexA (attp40)	Gift from Zlatic lab	N/A
Mi{Trojan-LexA-QFAD.2}Gad1	Bloomington Drosophila Stock Center	RRID: BDRC_60324
20xUAS-IVS-CsChrimson::mVenus (attp2)	Bloomington Drosophila Stock Center	RRID: BDRC_55134
20xUAS-IVS-CsChrimson::mVenus (attP18)	Bloomington Drosophila Stock Center	RRID: BDRC_55136
20xUAS-IVS-CsChrimson::mVenus (attP18);;R72F11-Gal4 (attp2)	Bloomington Drosophila Stock Center	RRID: BDRC_79599
13xLexAop2-IVS-CsChrimson::mVenus (attP18)	Bloomington Drosophila Stock Center	RRID: BDRC_55137
13xLexAop2-IVS-CsChrimson::tdTomato (attP18)	Gift from Rubin lab	N/A
13xLexAop2-IVS-CsChrimson::tdTomato (vk000005)	Bloomington Drosophila Stock Center	RRID: BDRC_82183
20xUAS(FRT.stop)CsChrimson.mVenus(attP18), pBPhsFlp2::Pest (AttP3)	Gift from Rubin lab	N/A
hs(KDRT.stop)FLP (attP18)	Bloomington Drosophila Stock Center	RRID: BDRC_67091
20xUAS(FRT.stop)-CsChrimson::mVenus	Gift from Rubin lab	N/A
UAS-TeTxLC.tnt	Bloomington Drosophila Stock Center	RRID: BDRC_28838
20xUAS-TTS-Shibire^{ts1}-p10(vk00005)	Bloomington Drosophila Stock Center	PRID: BDRC_66600
10xUAS-IVS-mry::GFP (attP18)	Gift from Rubin lab	N/A
13xLexAop-dsRed (attP2)	Gift from Rubin lab	N/A
20xUAS-IVS-GCaMP6s (vk00005)	Bloomington Drosophila Stock Center	RRID: BDRC_4279
20xLexAop-IVS-Syn21-GCaMP6s (su(HW)attP8)	Gift from Rubin lab	N/A
20xUAS-Syn21-opGCaMP6s (su(Hw)attP8)	Gift from Rubin lab	N/A
10xUAS-Syn21-CsChrimson88::tdTomato(attP18)	Gift from Rubin lab	N/A
HMS02355	Bloomington Drosophila Stock Center	RRID: BDRC_41958
HMC03388	Bloomington Drosophila Stock Center	RRID: BDRC_51817
JF02989	Bloomington Drosophila Stock Center	RRID: BDRC_28353
HMC02975	Bloomington Drosophila Stock Center	RRID: BDRC_50608
HMC03643	Bloomington Drosophila Stock Center	RRID: BDRC_52903
Software and algorithms		
FIJI	https://fiji.sc/	RRID: SCR_002285
MATLAB	MathWorks	RRID: SCR_001622
CATMAID	https://catmaid.readthedocs.org/	RRID: SCR_006278
Multi Worm Tracker	http://sourceforge.net/projects/mwt	N/A
ZEN	Carl Zeiss Microscopy	Version 2.1 (blue edition)

Affinity Designer	Affinity	Version 1.10.5
ScanImage	MBF Bioscience	N/A

Fly stocks and maintenance

All *D. melanogaster* stock lines used in this study were raised on Bloomington Drosophila Stock Center cornmeal food. Flies were maintained in a humidity- and temperature-controlled chamber kept at 18°C or 25°C, 40% humidity, and set to a 12-hour light/dark cycle. All crosses for experiments were reared at 25°C and 40% humidity.

Fly genotypes used in experiments

-Main figures

Fig.	Panel	Labels	Genotypes
1	A	Basin	*20xUAS-IVS-CsChrimson::mVenus/+;+; R72F11-Gal4/+*
1	A	Basin + SS04185	*20xUAS-IVS-CsChrimson::mVenus/+; R54B01-Gal4.AD/+; R46E07-Gal4.DBD/ R72F11-Gal4*
1	B, D-G	-	*20xUAS-IVS-CsChrimson::mVenus/+; +; R72F11-Gal4/+*
1	B, D-G	SS04185	*20xUAS-IVS-CsChrimson::mVenus/+; R54B01-Gal4.AD/+; R46E07-Gal4.DBD/R72F11-Gal4*
1	C	- / UAS-CsChrim	*20xUAS-IVS-CsChrimson::mVenus/+;;*
1	C	SS04185 / UAS-CsChrim	*20xUAS-IVS-CsChrimson::mVenus/+; R54B01-Gal4.AD/+; R46E07-Gal4.DBD/+*
1	C	- / 72F11>CsChrim	*20xUAS-IVS-CsChrimson::mVenus/+; +; R72F11-Gal4/+*
1	C	SS04185 / 72F11>CsChrim	*20xUAS-IVS-CsChrimson::mVenus/+; R54B01-Gal4.AD/+; R46E07-Gal4.DBD/R72F11-Gal4*
2	A		*10xUAS-IVS-mry::GFP/+; R54B01-Gal4.AD/+; R46E07-Gal4.DBD/+*
2	B	control	*20xUAS-IVS-CsChrimson::mVenus/+; R54B01-Gal4.AD/+; R46E07-Gal4.DBD/R72F11-Gal4*
2	B	MB>KZip+	*20xUAS-IVS-CsChrimson::mVenus/+; R13F02-LexA,LexAop-KZip^{+}/R54B01-Gal4.AD; R72F11-Gal4/R46E07-Gal4.DBD*
2	C-E	MB>KZip+	*20xUAS-IVS-CsChrimson::mVenus/+; R13F02-LexA,LexAop-KZip^{+}/+; R72F11-Gal4/+*
2	C-E	SS04185	*20xUAS-IVS-CsChrimson::mVenus/+; R54B01-Gal4.AD/+; R46E07-Gal4.DBD/R72F11-Gal4*
2	C-E	MB>KZip+, SS04185	*20xUAS-IVS-CsChrimson::mVenus/+; R13F02-LexA,LexAop-KZip^{+}/R54B01-Gal4.AD; R72F11-Gal4/R46E07-Gal4.DBD*
2	F-H	-	*w+, hs(KDRT.stop)FLP/13xLexAop2-IVS-CsChrimson::tdTomato; R54B01-Gal4.AD/72F11-LexA;20xUAS-(FRT.stop)-CsChrimson::mVenus/R46E07-Gal4.DBD*
2	F-H	SS04185-DN	*w+, hs(KDRT.stop)FLP/13xLexAop2-IVS-CsChrimson::tdTomato; R54B01-Gal4.AD/72F11-LexA;20xUAS-(FRT.stop)-CsChrimson::mVenus/R46E07-Gal4.DBD*
3	D, E		*10xUAS-IVS-mry::GFP/+; R54B01-Gal4.AD/+; R46E07-Gal4.DBD/+*
3	F		*w; R54B01-Gal4.AD/R72F11-LexA; R46E07-Gal4.DBD/13xLexAop2-IVS-CsChrimson::tdTomata, 20xUAS-IVS-GCaMP6s*
3	H		*w; R54B01-Gal4.AD/R71A10-LexA; R46E07-Gal4.DBD/13xLexAop2-IVS-CsChrimson::tdTomata, 20xUAS-IVS-GCaMP6s*

3	J		*w; R54B01-Gal4.AD/ppk1.9-LexA; R46E07-Gal4.DBD/13xLexAop2-IVS-CsChrimson::tdTomata, 20xUAS-IVS-GCaMP6s*
4	B		*w; R72F11-LexA/R54B01-Gal4.AD; 13xLexAop-CsChrimson, 20xUAS-IVS-UAS-GCaMP6s/R46E07-Gal4.DBD*
4	C		*w; R71A10-LexA/R54B01-Gal4.AD; 13xLexAop-CsChrimson, 20xUAS-IVS-UAS-GCaMP6s/R46E07-Gal4.DBD*
4	D		*w; R72F11-LexA/+; 13xLexAop2-IVS -CsChrimson::tdTomato, 20xUAS-IVS-UAS-GCaMP6s/R71A10-Gal4*
4	E	A00c	*w; R72F11-LexA/+; 13xLexAop2-IVS -CsChrimson::tdTomato, 20xUAS-IVS-UAS-GCaMP6s/R71A10-Gal4*
4	E	SS04185	*w; R72F11-LexA/R54B01-Gal4.AD; 13xLexAop2-IVS -CsChrimson::tdTomato, 20xUAS-IVS-UAS-GCaMP6s/R46E07-Gal4.DBD*
5	A		*10xUAS-mryGFP; R54B01-Gal4.AD/13x-LexAop-dsRed; R46E07-Gal4.DBD/ Mi{Trojan-LexA-QFAD.2}Gad1*
5	B-D	-	*13xLexAop2-IVS-CsChrimson::mVenus;R72F11-lexA/+; HMS02355/+*
5	B-D	SS04185	*13xLexAop2-IVS-CsChrimson::mVenus; R72F11-lexA/R54B01-Gal4.AD; HMS02355/R46E07-Gal4.DBD*
6	A-F	-	*13xLexAop2-IVS-CsChrimson::mVenus; R72F11-LexA/+; UAS-TeTxLC.tnt /+*
6	A-F	SS04185	*13xLexAop2-IVS-CsChrimson::mVenus; R72F11-LexA/R54B01-Gal4.AD; UAS-TeTxLC.tnt/R46E07-Gal4.DBD*
7	A, B	-	*20xUAS-IVS-CsChrimson::mVenus/+; ; R72F11-Gal4/+*
7	A, B	GABA-B-R1[1]	*20xUAS-IVS-CsChrimson::mVenus/+; ; R72F11-Gal4/UAS-HMC03388*
7	A, B	GABA-B-R1[2]	*20xUAS-IVS-CsChrimson::mVenus/+; ; R72F11-Gal4/UAS-JF02989*
7	A, B	GABA-B-R2	*20xUAS-IVS-CsChrimson::mVenus/+; ; R72F11-Gal4/UAS-HMC02975*
7	A, B	GABA-A-R	*20xUAS-IVS-CsChrimson::mVenus/+; ; R72F11-Gal4/UAS-HMC03643*
7	C	Basin activation	*20xUAS-Syn21-opGCaMP6s,10XUAS-Syn21-CsChrimson88::tdTomato/+;CyO/+;TM6/R72F11-Gal4*
7	C	SS04185 and Basin activation	*20xUAS-Syn21-opGCaMP6s,10XUAS-Syn21-CsChrimson88::tdTomato/+;CyO/R54B01-Gal4.AD;R72F11-Gal4/R46E07-Gal4.DBD*
8	A-D	-	*20xUAS-IVS-CsChrimson::mVenus/+; R72F11-Gal4.AD/+; R38H09-Gal4.DBD/+*
8	A-D	SS04185	*20xUAS-IVS-CsChrimson::mVenus/+; R72F11-Gal4.AD/R54B01-Gal4.AD; R38H09-Gal4.DBD/R46E07-Gal4.DBD*
8	E-H	-	*20xUAS-IVS-CsChrimson::mVenus/+; R72F11-Gal4.AD/+; R57F07-Gal4.DBD/+*
8	E-H	SS04185	*20xUAS-IVS-CsChrimson::mVenus/+; R72F11-Gal4.AD/R54B01-Gal4.AD; R57F07-Gal4.DBD/R46E07-Gal4.DBD*

-Supplementary figures

Fig.	Panel	Labels	Genotypes
1	A-D	-	*20xUAS-IVS-CsChrimson::mVenus/+;;*
1	A-D	SS04185	*20xUAS-IVS-CsChrimson::mVenus/+; R54B01-Gal4.AD/+; R46E07-Gal4.DBD/+*
1	E-H	-	*20xUAS-IVS-CsChrimson::mVenus/+; +; R72F11-Gal4/+*
1	E-H	SS04185	*20xUAS-IVS-CsChrimson::mVenus/+; R54B01-Gal4.AD/+; R46E07-Gal4.DBD/R72F11-Gal4*
1	I	- / UAS-CsChrim	*20xUAS-IVS-CsChrimson::mVenus/+;;*
1	I	SS04185 / UAS-CsChrim	*20xUAS-IVS-CsChrimson::mVenus/+; R54B01-Gal4.AD/+; R46E07-Gal4.DBD/+*
1	I	- / 72F11>CsChrim	*20xUAS-IVS-CsChrimson::mVenus/+; +; R72F11-Gal4/+*

1	I	SS04185 / 72F11>CsChrim	*20xUAS-IVS-CsChrimson::mVenus/+; R54B01-Gal4.AD/+; R46E07-Gal4.DBD/R72F11-Gal4*
2	A		*20xUAS-IVS-CsChrimson::mVenus/+; R13F02-LexA,LexAop-KZip^{+}/R54B01-Gal4.AD; R72F11-Gal4/R46E07-Gal4.DBD*
2	B, C	MB>Kzip+	*20xUAS-IVS-CsChrimson::mVenus/+; R13F02-LexA,LexAop-Kzip^{+}/+; R72F11-Gal4/+*
2	B, C	SS04185	*20xUAS-IVS-CsChrimson::mVenus/+; R54B01-Gal4.AD/+; R46E07-Gal4.DBD/R72F11-Gal4*
2	B, C	MB>Kzip+, SS04185	*20xUAS-IVS-CsChrimson::mVenus/+; R13F02-LexA,LexAop-Kzip^{+}/R54B01-Gal4.AD; R72F11-Gal4/R46E07-Gal4.DBD*
2	D, E	control	*20xUAS-IVS-CsChrimson::mVenus/+; +; R72F11-Gal4/+*
2	D, E	MB247	*20xUAS-IVS-CsChrimson::mVenus/+; R54B01-Gal4.AD/+; R46E07-Gal4.DBD/R72F11-Gal4*
2	F, G		*w+, hs(KDRT.stop)FLP/13xLexAop-CsChrimson::tdTomato; R54B01-Gal4.AD/72F11-LexA;20xUAS-(FRT.stop)-CsChrimson::mVenus/R46E07-Gal4.DBD*
2	H-J	control	*w+, hs(KDRT.stop)FLP/13xLexAop-CsChrimson::tdTomato; R54B01-Gal4.AD/72F11-LexA; 20xUAS-(FRT.stop)-CsChrimson::mVenus/R46E07-Gal4.DBD*
2	H-J	SS04185-DN	*w+, hs(KDRT.stop)FLP/13xLexAop-CsChrimson::tdTomato; R54B01-Gal4.AD/72F11-LexA; 20xUAS-(FRT.stop)-CsChrimson::mVenus/R46E07-Gal4.DBD*
4		SeIN128 (Basin activation)	*w; R72F11-LexA/R54B01-Gal4.AD; 13xLexAop2-IVS -CsChrimson::tdTomato, 20xUAS-IVS- GCaMP6s/R46E07-Gal4.DBD*
4		SeIN128 (A00c activation)	*w; R71A10-LexA/R54B01-Gal4.AD; 13xLexAop2-IVS -CsChrimson::tdTomato, 20xUAS-IVS-GCaMP6s/R46E07-Gal4.DBD*
4		A00c (Basin activation)	*w; R72F11-LexA/+; 13xLexAop2-IVS -CsChrimson::tdTomato, 20xUAS-IVS-GCaMP6s/R71A10-Gal4*
5	A, B		*10xUAS-IVS-mry::GFP/+; R54B01-Gal4.AD/+; R46E07-Gal4.DBD/+*
6	A-G	-	*13xLexAop2-IVS-CsChrimson::mVenus; R72F11-LexA/+; 20xUAS-TTS-Shibire^{ts1}/+*
6	A-G	SS04185	*13xLexAop2-IVS-CsChrimson::mVenus; R72F11-LexA/R54B01-Gal4.AD; 20xUAS-TTS-Shibire^{ts1}/R46E07-Gal4.DBD*
7	A-D	-	*20xUAS-IVS-CsChrimson::mVenus/+; ; R72F11-Gal4/+*
7	A-D	GABA-B-R1^{1}	*20xUAS-IVS-CsChrimson::mVenus/+; ; R72F11-Gal4/UAS-HMC03388*
7	A-D	GABA-B-R1^{2}	*20xUAS-IVS-CsChrimson::mVenus/+; ; R72F11-Gal4/UAS-JF02989*
7	A-D	GABA-B-R2	*20xUAS-IVS-CsChrimson::mVenus/+; ; R72F11-Gal4/UAS-HMC02975*
7	A-D	GABA-A-R	*20xUAS-IVS-CsChrimson::mVenus/+; ; R72F11-Gal4/UAS-HMC03643*
7	E	Basin activation	*20xUAS-Syn21-opGCaMP6s,10XUAS-Syn21-CsChrimson88::tdTomato/+;CyO/+;TM6/R72F11-Gal4*
7	F	Basin + SeIN128	*20xUAS-Syn21-opGCaMP6s,10XUAS-Syn21-CsChrimson88::tdTomato/+;CyO/R54B01-Gal4.AD;R72F11-Gal4/R46E07-Gal4.DBD*
8	A, C	Basin-2	*20xUAS-IVS-CsChrimson::mVenus/+; R72F11-Gal4.AD/+; R38H09-Gal4.DBD/+*
8	B, C	Basin-4	*20xUAS-IVS-CsChrimson::mVenus/+; R72F11-Gal4.AD/+; R57F07-Gal4.DBD/+*
8	D, E	-	*20xUAS-IVS-CsChrimson::mVenus/+; R72F11-Gal4.AD/+; R38H09-Gal4.DBD/+*
8	D, E	SS04185	*20xUAS-IVS-CsChrimson::mVenus/+; R72F11-Gal4.AD/R54B01-Gal4.AD; R38H09-Gal4.DBD/R46E07-Gal4.DBD*
8	F, G	-	*20xUAS-IVS-CsChrimson::mVenus/+; R72F11-Gal4.AD/+; R57F07-Gal4.DBD/+*
8	F, G	SS04185	*20xUAS-IVS-CsChrimson::mVenus/+; R72F11-Gal4.AD/R54B01-Gal4.AD; R57F07-Gal4.DBD/R46E07-Gal4.DBD*

505

Behavior assay

Larvae were kept in the dark at 25°C for four days to grow to the 3rd instar stage. To optogenetically stimulate neurons, larvae were raised on fly food plates with 0.2 mM trans-retinal (Toronto Research Chemicals, R240000). Before the experiment, food plates with larvae were rinsed with a 15% sucrose solution to separate the larvae from the food. Larvae were then moved to a sieve, washed with water, dried, and placed evenly on 2% agar plates. The agar plate with animals were placed under a camera in the arena of the behavior rig.

- **Behavior apparatus**

The behavior rig consisted of several apparatuses, including a C-MOS camera (Grasshopper Camera USB3, GS3-U3-41C6M-C, FLIR), infrared illumination, a 610-nm light-emitting diode (LED) for optogenetic manipulations, a computer, and a heating panel. Both the camera and LED source were controlled by the computer. LED stimuli were controlled by customized software while larval behaviors were recorded using the Multi-Worm Tracker (MWT) software (Swierczek et al., 2011). These two pieces of software were synchronized in the behavior assay to precisely deliver the stimulation during specified time windows.

- **Optogenetic stimulation**

Before delivering optogenetic stimulation, larvae were placed in the arena for 45 s. Subsequently, two 30-s 624-nm LED stimuli were presented successively with a 30-s interval between them. The LED intensity used in each experiment is shown below.

Figure number	**Optogenetic stimulation irradiance ($\mu W/mm^2$)**
Figure 1	0.84
Figure 1 – supplementary figure-1	0.84
Figure 2C-E	5.9
Figure 2F-H	1.8
Figure 2 – supplementary figure-1B-C	5.9
Figure 2 – supplementary figure-1D-E	0.84
Figure 2 – supplementary figure-1H-J	1.8
Figure 5B-D	1.8
Figure 6	1.8
Figure 6 – supplementary figure-1	1.8
Figure 7A-B	0.84
Figure 7 – supplementary figure-1A-D	0.84
Figure 8A-D	3.9
Figure 8E-H	1.8
Figure 8 – supplementary figure-1A-C	1.8
Figure 8 – supplementary figure-1D-E	3.9
Figure 8 – supplementary figure-1F-G	1.8

525

526 **Thermal stimulation**

527 To provide heat stimulation, we built thermal control systems with a proportional-integral-
528 derivative (PID) temperature controller (ITC-106VH, Inkbird), a solid-state relay for temperature
529 controllers (SSR-25A, Inkbird), a K-Type thermocouple to detect temperature, and a heat panel.
530 The thermal control system was connected to a custom-built incubator designed to maintain a
531 steady temperature inside the behavior rig at 32°C and warm the agar plates. The temperature of
532 the agar plates was monitored by a thermometer gun (62 MAX+ Compact Infrared Thermometer,
533 Fluke) before and after the experiment to verify the appropriate temperature for *shibire*^{ts1} to be
534 functional. Larvae were sealed in a plastic sieve and pre-heated in a water bath for 10 min to
535 reach 32°C before the test. In order to maintain the temperature above 30°C during the test, a
536 replica of the thermal control system mentioned above was installed in the behavior rig, and the
537 behavior rig was pre-heated overnight before any thermal experiment.
538 For *shibire*^{ts1} experiments with heat stimulation, during the first 5 s of the test, larvae were left on
539 the agar plates without LED stimulation. Subsequently, the larvae were optogenetically
540 stimulated with a 624-nm LED for 30 s.

541 **Behavior analysis**

542 Larvae were tracked in real-time using MWT software
543 (https://github.com/Ichoran/choreography). Objects that were tracked for less than 5 s or moved
544 less than one body length of a larva were rejected. The contour, spine, and center of mass were
545 generated and recorded by MWT as a function of time. From these tracking data, the key
546 parameters of larval motion were computed using specific Choreography (a component of the
547 MWT software package) variables tailored for *Drosophila* larvae (as opposed to *C. elegans*) as
548 described previously (Ohyama et al., 2013; Ohyama et al., 2015). We refer readers to the open-
549 source package for further details of the software implementations for the above calculations.

550 - **Behavior detection**

551 After extracting features from Choreography, we used an unsupervised machine learning
552 behavior classification algorithm to detect and quantify the following behaviors: hunching
553 (Hunch), head-bending (Turn), stopping (Stop), and peristaltic crawling (Crawl) as previously
554 reported (Masson et al., 2020). Escape rolling (Roll) was detected with a classifier developed
555 with Janelia Automatic Animal Behavior Annotator (JAABA) (Kabra et al., 2013; Ohyama et al.,

2015). JAABA transformed the MWT tracking data into a collection of 'per-frame' features and regenerated videos of the tracked larvae. Behaviors were then labeled manually frame-by-frame with these regenerated videos. We labeled roll, non-roll, and unknown frames in the randomly chosen ~10,000 frames to train the algorithm to correctly classify larval rolling behavior. This classifier, which has false negative and false positive rates of 7.4% and 7.8%, respectively (n=102), was utilized to detect rolling in this paper.

- **Behavior quantification**

The outputs of these behavior detection pipelines served as the input to a customized follow-up MATLAB-based analysis. Only the larvae being tracked fully during the stimulation window were selected for analysis. The percentages of animals performing given behaviors as well as their crawling speed in time series at a frame rate of 10 fps were plotted to depict the behavioral responses. To quantify the behavioral phenotype at the population level, the proportions of larvae that performed given behaviors at least once in the first 5 s after the onset of the stimulation were calculated in percentages. A collection of individual-level parameters (e.g., aggregated durations of rolling throughout the stimulation window, starts and ends of the first rolling event after stimulus onset, starts of the first crawling event after the first rolling event in the stimulation window) were generated and analyzed to describe the effects of stimulation on escape behaviors. Specifically, the starts of the first crawling events after the first rolling events were recorded as 30 s by default if larvae rolled but never initiated crawling during the stimulation window. Furthermore, the cumulative plots of the durations of each rolling event were contrasted to describe the event-level differences.

Larval dissections and immunohistochemistry

The CNSs of *Drosophila* larvae were dissected in phosphate-buffered saline (PBS). After dissection, tissues were fixed with 4% paraformaldehyde for 20 min, washed with PBS 3 times and then washed with 0.4% Triton X-100 in PBS (PBST) twice. Samples were incubated at room temperature with a blocking solution (5% normal goat serum [NGS]) for 1 h. Next, the samples were incubated with the primary antibody solutions at 4°C overnight. The primary antibodies were diluted at concentrations of 1:3000 for chicken anti-GFP; 1:1000 for rabbit anti-GFP and rabbit anti-dsRed; 1:50 for mouse nc82; and 1:20 for rat anti-DN-Cadherin, mouse anti-Fas2, mouse anti-choline acetyltransferase (ChAT), and rabbit anti-GLUT1 in 5% NGS. CNS samples were then incubated with a secondary antibody solution at 4°C overnight. The secondary

antibodies, including anti-chicken Alexa488, anti-rabbit Alexa488, anti-mouse Alexa568, anti-rabbit Alexa568, and anti-rat Alexa568, were all diluted at the concentration of 1:500. These samples were mounted in VECTASHIELD antifade mounting medium and imaged by a Zeiss LSM 710 confocal microscope with a 20x/NA0.8 objective lens (Zeiss) and Zen digital imaging software (Zeiss). All images were processed using Fiji software (https://imagej.new/Fiji, ImageJ, NIH Bethesda).

Two-photon calcium imaging assay

The CNSs of third instar larvae were dissected out in cold Baines external physiological saline (135 mM NaCl, 5 mM KCl, 5 mM TES, 36 mM sucrose, 2 mM $CaCl_2$-$2H_2O$, 4 mM $MgCl_2$-$6H_2O$, pH 7.15), and secured on a poly-L-lysine coated cover glass placed in a small Sylgard plate.

Functional calcium imaging experiments were performed on a customized two-photon microscope equipped with a Galvo-Resonant Scanner (Cambridge) controlled by Scanimage software (mbf BIOSCIENCE) using a 40x/0.80NA water immersion objective (LUMPlanFL, Olympus). A Mai Tai®, Ti:Sapphire Ultrafast Laser (Spectra Physics) tuned to 925 nm was used for excitation of GCaMP protein. Fluorescence signals were collected with photomultiplier tubes (Hamamatsu) after bandpass filtering. Images were acquired by the Galvo-Resonant Scanner for a single plane of the CNS.

Each larva was stimulated by a 620-nm LED (Thorlabs) through the objective three times with a 30-s interval between periods of stimulation. Every stimulus consisted of a 30-ms pulse given every 100 ms for a total of 1 s. Light intensity was measured to be 0.8-1.4 mW/mm2. Images were acquired at a resolution of 512 x 512 pixels with a frame rate of 30 fps. Fluorescence intensities were averaged to 6 fps and processed in FIJI, and analyzed in MATLAB with customized scripts. Regions of interest (ROI) were determined by the standard deviation of the full recording. $\Delta F=(F-F_0)/F_0$. F_0 is the average of images taken 10 frames (i.e., 1.7 s) before stimulation. F is the mean value of the fluorescence in the ROI averaged every 5 frames from the start of the 5-s period before stimulation to end of the 15-s period after the onset of each stimulation. For each larva, ΔF is obtained through averaging the ΔF during the three stimulation periods. The peak ΔFs were the maximal values selected from the onset of stimulation to 15 s after stimulus onset.

Statistics

The probabilities for each response were analyzed by Chi-square tests. For the other parameters, when multiple groups were tested, their normality was examined first. If the normality assumption was rejected, Kruskal-Wallis tests were performed for multiple group variance comparisons, followed by multiple-comparison-corrected Wilcoxon–Mann–Whitney tests as post hoc pairwise comparisons. If normality was met, analysis of variance (ANOVA) was performed for variance comparisons and multiple-comparison-corrected student's t-tests were utilized for pairwise comparisons. For two group comparisons, the Wilcoxon–Mann–Whitney test was conducted if the normality assumption was offended, and the student's t-test was applied if normality was met. All analyses were conducted with MATLAB.

Data availability statement

The original contributions presented in this study are included in the article/supplemental material; further inquiries may be directed to the corresponding author.

Conflict of interests

The authors declare that the research was conducted in the absence of any commercial or financial relationships that could be construed as a potential conflict of interests.

Author contributions

Conceptualization, J.Z. and T.O. Writing – Original Draft, J.Z. and T.O; Writing – Review & Editing, J.Z., J-C.B., and T.O. Formal Analysis, J.Z., J-C.B., and T.O. Performing experiments, J.Z., J-C.B., J.N., Y.Q.Z., and T.O. Supervision, T.O.

Funding

This work was funded by McGill University, the National Sciences and Engineering Research Council (NSERC, RGPIN/04781-2017), the Canadian Institute of Health Research (CIHR, PTJ-376836), the Fonds de recherche du Quebéc - Nature et technologies (FRQNT, 2019-N-25523), and the Canada Foundation for Innovation (CFI, CFI365333). J-C.B was supported by Fonds de recherche du Quebéc-Santé (FRQS) graduate training award.

Acknowledgements

We thank J.W. Truman, A. Cardona and M. Zlatic for generating and sharing the split Gal4 lines. J. Truman and M. Zlatic for constructive inputs on the project. Confocal images were collected at the McGill University Advanced Bio Imaging Facility (ABIF), RRID:SCR_017697. We also thank the Bloomington stock center for providing fly stocks. We thank members of Ohyama lab for critical comments on the manuscript.

Inclusion and diversity

One or more of authors of this paper self-identifies as a member of the LGBTYQ+ community.

Figure legends:

Figure 1. Activation of SS04185 inhibits rolling evoked by activation of Basin neurons

(A) Ethograms of Basin activation (top panel) and co-activation of SS04185 and Basins (bottom panel). Each row represents an individual larva. Pink, blue, green, orange, and purple lines represent bouts of rolling, turning, crawling, backward crawling, and hunching. The red bar and dashed lines indicate the time window during which neural activation was present. Genotypes: *20xUAS-IVS-CsChrimson::mVenus/+;+; R72F11-Gal4/+* (top); *20xUAS-IVS-CsChrimson::mVenus/+; R54B01-Gal4.AD/+; R46E07-Gal4.DBD/ R72F11-Gal4* (bottom). Genotypes in (B, D-G) are the same as those mentioned here.

(B) Time series of rolling probabilities of larvae during co-activation of SS04185 and Basins (red) and activation of Basins alone (black), as well as crawling speed of larvae during activation of Basins alone (green). Shaded areas represent 95% confidential intervals for rolling probabilities. The red bar and dashed lines denote the optogenetic stimulation window.

(C) Rolling probabilities of larvae with activation of different neurons. Error bars represent the 95% confidence interval. Genotypes from left to right: 1) *20xUAS-IVS-CsChrimson::mVenus/+; ; ,* 2) *20xUAS-IVS-CsChrimson::mVenus/+; R54B01-Gal4.AD/+; R46E07-Gal4.DBD/+*, 3) *20xUAS-IVS-CsChrimson::mVenus/+; ; R72F11-Gal4/+*, 4) *20xUAS-IVS-CsChrimson::mVenus/+; R54B01-Gal4.AD/+; R46E07-Gal4.DBD/ R72F11-Gal4.* n = 120, 118, 231, 155 from left to right. Statistics: Chi-square test, $\chi^2 = 0$, $p > 0.05$ for the first two groups; $\chi^2 = 83.85$, $p < 0.001$ for the last two groups; and $\chi^2 = 365.51$, $p < 0.001$ for the comparison between the first two groups and the last two groups.

(D) Cumulative plot of rolling duration. Statistics: Mann-Whitney test, $p < 0.001$, n = 652, 120.

(E) A violin plot showing start of first rolling bout for each larva during stimulation. Statistics: Mann-Whitney test, $p = 0.027$, n = 225, 89.

(F) A violin plot displaying end of first rolling bout for each larva during stimulation. Statistics: Mann-Whitney test, $p < 0.001$, n = 225, 89.

(G) A violin plot presenting start of first crawling bout for each larva during stimulation. Statistics: Mann-Whitney test, $p < 0.001$, n = 214, 70.

$^{**}p < 0.01$, $^{***}p < 0.001$.

Figure 2. SS04185-DN, but not SS04185-MB, inhibits rolling when co-activated with Basins

(A) Morphology of SS04185 neurons. GFP, grey (left), green (right); nc82, magenta. Anterior, up; dorsal view; scale bar, 100 µm. Genotype: 10x*UAS-IVS-mry::GFP/+; R54B01-Gal4.AD/+; R46E07-Gal4.DBD/+*.

(B) Kenyon cells are less labeled in SS04185 with MB>Kipper Zipper. CsChrimson expression in Kenyon cells of SS04185 in Control and SS04185 with Killer Zipper in mushroom body (MB). GFP, grey (left), green (right); nc82, magenta. Anterior, up; dorsal view; scale bar, 20 µm. Genotype: *20xUAS-IVS-CsChrimson::mVenus/+; R54B01-Gal4.AD/+; R46E07-Gal4.DBD/+* (Control); *20xUAS-IVS-CsChrimson::mVenus/+; R13F02-LexA,LexAop-KZip^{+}/R54B01-Gal4.AD; R72F11-Gal4/R46E07-Gal4.DBD* (MB>KZip^{+}).

(C) Rolling probabilities of larvae with activation of SS04185 reduce the expression of CsChrimson in mushroom body (MB) neurons. Error bars, 95% confidence interval. n = 78, 55, 100 from left to right. Statistics: Chi-square test, $\chi^2 = 2.32$, $p > 0.05$ for the two groups with SS04185 expression; $\chi^2 = 37.50$, $p < 0.001$ for the comparison between the two groups on the left; $\chi^2 = 70.45$, $p < 0.001$ for the comparison between the groups with *MB>KZip^{+}* expression which reduce expression of CsChrimson in MB. Genotypes: *20xUAS-IVS-CsChrimson::mVenus/+; R13F02-LexA,LexAop-KZip^{+}/+; R72F11-Gal4/+* (black); *20xUAS-IVS-CsChrimson::mVenusR54B01-Gal4.AD/+; R46E07-Gal4.DBD/R72F11-Gal4* (dark red); *20xUAS-IVS-CsChrimson::mVenus/+; R13F02-LexA,LexAop-KZip^{+}/R54B01-Gal4.AD; R72F11-Gal4/R46E07-Gal4.DBD* (red). Genotypes in (D-E) are the same as mentioned here.

(D) Cumulative plot of rolling duration. Statistics: Kruskal-Wallis test: H = 8.28, $p = 0.016$; Bonferroni-corrected Mann-Whitney test, $p > 0.05$ for all pairwise post-hoc tests, n = 103, 20, 27 from left to right.

(E) A violin plot of start of first crawling bout for each larva during stimulation. Statistics: Kruskal-Wallis test: H = 15.02, $p < 0.001$; Bonferroni-corrected Mann-Whitney test, $p > 0.05$ for the two groups with SS04185 expression; $p < 0.001$ for the comparison between the group without SS04185 expression and the groups with full SS04185 expression, n = 65, 20, 7 from left to right.

(F) The probabilities of larval rolling during first 5 s of stimulation. Error bars, 95% confidence interval. n = 101, 126. Statistics: Chi-square test, $\chi^2 = 4.27$, $p = 0.039$. Genotype: *13xLexAop2-IVS-CsChrimson::tdTomato/w^{+}, hs-FLP; R54B01-Gal4.AD/72F11-LexA; 20XUAS-(FRT.stop)-CsChrimson::mVenus/R46E07-Gal4.DBD*. Genotypes in (G-H) are the same as mentioned here.

(G) Cumulative plot of rolling duration. Statistics: Mann-Whitney test, $p < 0.001$, n = 350, 473.
(H) A violin plot of start of first crawling bout for each larva during stimulation. Statistics: Mann-Whitney test, $p < 0.001$, n = 97, 120.
$^{**}p < 0.01$, $^{***}p < 0.001$.

Figure 3. SS04185-DN is identical to SeIN128

(A) TEM neuron reconstruction of SeIN128 neurons. Left panel: anterior, up; dorsal view. Right panel: anterior, up; dorsal, right; lateral view. Red dots, presynaptic sites. Cyan dots, postsynaptic sites.
(B) A transverse section of larval CNS from EM reconstruction data. SeIN128 (green), Basins (blue), and A00c (orange) are located in ventromedial tract (VM). mdIV, red; magenta, neural tracts. DM, dorsomedial tract; VM, ventromedial tract. Dorsal, up; anterior view; scale bar, 1 µm.
(C) Cartoon generated based on transverse section of SeIN128, Basin-1 to Basin-4, A00c, and mdIV from EM neuron reconstruction data and (D). Nerve tracts are shown in magenta. Dorsal, up; posterior view. DM, dorsomedial tract; VM, ventromedial tract; CI, central-intermediate tract; CL, central-lateral tract; DL, dorsolateral tract; VL, ventrolateral tract. SeIN128, green; Basin-1 to Basin-4, blue; A00c, orange; mdIV, red.
(D) SS04185-expressing neurons co-stained with N-Cadherin. A cell body of SS04185-Descending neuron located in ventral part of the subesophageal zone (SEZ). SS04185, Green; N-Cadherin, magenta. Anterior, up; left, dorsal view; right, longitudinal section; scale bar, 100 µm. Genotype: 10x*UAS-IVS-mry::GFP/+; R54B01-Gal4.AD/+; R46E07-Gal4.DBD/+*. SS04185, Green; Cadherin, magenta. Anterior, left, dorsal, up; lateral view; scale bar, 100 µm.
(E) Transverse section of SS04185-DN co-stained with Fas2. SS04185-DN located at ventromedial tract (VM). SS04185, Green; Fas2, magenta. Dorsal, up; posterior view; scale bar, 20 µm. DM, dorsomedial tract; VM, ventromedial tract; CI, central-intermediate tract; CL, central-lateral tract; DL, dorsolateral tract; VL, ventrolateral tract. Genotype: 10x*UAS-IVS-mry::GFP/+; R54B01-Gal4.AD/+; R46E07-Gal4.DBD/+*.
(F, H, J) SS04185-DN co-localized with Basins or A00C neuron tract but not MdIV. SS04185, Green; Basins (F), A00c (H) or mdIV (J), magenta;. Genotype: *w; R54B01-Gal4.AD/R72F11-LexA(F) 71A10-LexA(H) or ppk1.9-LexA(J); R46E07-Gal4.DBD/13xLexAop2-IVS-*

CsChrimson::tdTomato,20xUAS-IVS-GCaMP6s. Top panel: anterior, up; dorsal view; scale bar, 10 µm. Bottom panel: dorsal, up; posterior view; scale bar, 5 µm.

(G, I, K) SeIN128, Basin-2, A00c or mdIV morphologies from the TEM neural reconstruction. Anterior, up; dorsal view. SS04185, green; Basin-2, blue; A00C, orange; mdIV, red.

Figure 4. SeIN128 receives input from Basin and A00c neurons

(A) Summary of the connectivity between SeIN128 and the escape circuit. SeIN128 receives inputs from Basin-2 and A00c and provide feedback to Basin-2 and A00c. Synapse number shown next to connection arrows, where line width is proportional to synapse number. All connections in the ventral nerve cord are shown except unilateral synapses, <5 synapses, between neurons. Each polygon represents a pair of the indicated neuron and segment (segment number is shown under the neuron name). SeIN128, green; Basin-2, blue; A00c, orange; mdIV, red.

(B, C) SeIN128 is functionally downstream of Basins (B) or A00c (C). Calcium transients, $\Delta F/F_0$ traces of GCaMP6s in SeIN128 axons (black line, mean) during 610-nm optogenetic activation of Basins at various intensities. Vertical gray line represents optogenetic activation. Genotype: *w; R72F11-LexA (B) or R71A10-LexA (C) /R54B01-Gal4.AD; 13xLexAop2-IVS—CsChrimson::tdTomato, 20xUAS-IVS-GCaMP6s/R46E07-Gal4.DBD.*

(D) A00c responses are faster and stronger than SeIN128 responses during activation of Basins. Calcium transients (black line, mean; gray line, single recording) represented by $\Delta F/F_0$ in A00c by of 610-nm optogenetic activation of Basins at various intensities. Genotype: *w; R72F11-LexA/+; 13xLexAop2-IVS-CsChrimson::tdTomato, 20xUAS-IVS-GCaMP6s/R71A10-Gal4.*

For (B) to (D), irradiances from left to right are 0.04, 0.1, 0.3, 0.5, and 1.4 µW/mm^2. For each irradiance (n = 6), individual traces are shown with gray lines whereas the average of individuals is shown in black. The shaded gray area indicates the period of optogenetic activation (0 to 1 s).

(E) The timing of the peak $\Delta F/F_0$ correlated with the identity of the neurons but not the peak $\Delta F/F_0$ value. SeIN128 neurons are shown as orange dots, whereas A00c is shown as a green dot.

Figure 5. SeIN128 is GABAergic and negatively controls rolling

(A) Immunostaining of SeIN128 cell body (green) and GABAergic neuron (magenta). Genotype: *10xUAS-IVS-mryGFP; R54B01-Gal4.AD/13xLexAop-dsRed; R46E07-Gal4.DBD/Trojan-GAD-*

T2A-LexA. White triangles indicate locations of SeIN128 cell bodies. Anterior, up; dorsal view; scale bar, 10 μm.

(B) Time series of rolling probabilities of larvae with Basin activation (black), or VGAT RNAi in SS04185 and Basin activation (red). The red bar and dashed lines display the window of optogenetic stimulation eliciting larval escape responses. Shaded areas show 95% confidential intervals of rolling probabilities. Genotypes: *13xLexAop2-IVS-CsChrimson::mVenus; R72F11-LexA/+; HMS02355/+* (black); *13xLexAop2-IVS-CsChrimson::mVenus; R72F11-LexA/R54B01-Gal4.AD; HMS02355/R46E07-Gal4.DBD* (red). Genotypes in (C, D) are the same as mentioned here.

(C) Binned larval rolling probabilities during first 5 s of stimulation in (A). Error bars, 95% confidence interval. n = 110, 73. Statistics: Chi-square test, $\chi^2 = 9.34$, $p < 0.001$.

(D) Cumulative plot of rolling duration. Statistics: Mann-Whitney test, $p = 0.015$, n = 55, 73.

$^{**}p < 0.01$, $^{***}p < 0.001$.

Figure 6. Inhibition of SeIN128 prolongs rolling and delays initiation of crawling

(A) Time series of rolling probabilities of larvae with Basin activation (black), or SS04185 inhibition and Basin activation (red). Shaded regions show 95% confidential intervals of rolling probabilities. Genotypes: *13xLexAop2-IVS-CsChrimson::mVenus; R72F11-LexA/+; UAS-TeTxLC.tnt/+* (black); *13xLexAop2-IVS-CsChrimson::mVenus; R72F11-LexA/R54B01-Gal4.AD; UAS-TeTxLC.tnt/R46E07-Gal4.DBD* (red). Genotypes in (B-F) are the same as mentioned here.

(B) Rolling probabilities during first 5 s of stimulation in (A). Error bars, 95% confidence interval. n = 241, 164. Statistics: Chi-square test, $\chi^2 = 44.02$, $p < 0.001$.

(C) A violin plot of total time spent rolling for each individual larva during stimulation. Statistics: Mann-Whitney test, $p < 0.001$, n = 221, 258.

(D) Cumulative plot of rolling duration. Statistics: Mann-Whitney test, $p < 0.001$, n = 160, 154.

(E) A violin plot of end of first rolling bout for each larva during stimulation. Statistics: Mann-Whitney test, $p < 0.001$, n = 160, 154.

(F) A violin plot of start of first crawling bout for each larva during stimulation. Statistics: Mann-Whitney test, $p < 0.001$, n = 65, 105.

$^{**}p < 0.01$, $^{***}p < 0.001$.

Figure 7. SeIN128 sends feedback inhibition to Basins

(A) Rolling probabilities for larvae with GABAR-RNAi in their Basin neurons. From left to right, the genotypes are *20xUAS-IVS-CsChrimson::mVenus/+; ; R72F11-Gal4/+* (black), *20xUAS—IVS-CsChrimson::mVenus/+; ; R72F11-Gal4/UAS-HMC03388* (dark green), *20xUAS-IVS-CsChrimson::mVenus/+; ; R72F11-Gal4/UAS-JF02989* (light green), *20xUAS-IVS-CsChrimson::mVenus/+; ; R72F11-Gal4/UAS-HMC02975* (yellow), and 20x*UAS-IVS-CsChrimson::mVenus/+; ; R72F11-Gal4/UAS-HMC03643* (orange). Genotypes in (B) are the same as mentioned here. N = 320, 205, 159, 183, 182 from left to right. Statistics: Chi-square test, Bonferroni correction. GABA-B-R1^1 group: $\chi^2 = 8.76$, $p = 0.012$. GABA-B-R1^2 group: $\chi^2 = 24.70$, $p < 0.001$. GABA-B-R2 group: $\chi^2 = 25.77$, $p < 0.001$. GABA-A-R group: $\chi^2 = 16.29$, $p < 0.001$.

(B) Cumulative plot of rolling duration. Statistics: Kruskal-Wallis test: H = 69.52, $p < 0.001$; Bonferroni-corrected Mann-Whitney test, $p < 0.001$ for GABA-B-R1^2, GABA-B-R2, and GABA-A-R RNAi groups, n = 520, 488, 387, 582, 306 from left to right.

(C) Summary of peak $\Delta F/F_0$ in Basin axons with or without SeIN128 activation under various irradiances. Control groups shown in black are without SeIN128 activation while experimental groups shown in red are with SeIN128 activation. Statistics: Mann-Whitney test, $p > 0.05$ for irradiances of 0.04, 0.1, 1.4 μW/mm^2; $p = 0.016$ for irradiance of 0.3 μW/mm^2; $p = 0.032$ for irradiance of 0.5 μW/mm^2. Genotype: *20xUAS-Syn21-opGCaMP6s, 10xUAS-Syn21-CsChrimson88::tdTomato/+; CyO/+;R72F11-Gal4/TM6* (black); *20xUAS-Syn21-opGCaMP6s,10xUAS-Syn21-CsChrimson88::tdTomato/+;CyO/R54B01-Gal4.AD;R72F11-Gal4/R46E07-Gal4.DBD* (red).

$^{**}p < 0.01$, $^{***}p < 0.001$.

Figure 8. SeIN128 inhibits rolling elicited by both Basin-2 and Basin-4 activation

(A) Binned larval rolling probabilities during the first 5 s of stimulation. Error bars, 95% confidence interval. n = 81, 119. Statistics: Chi-square test, $\chi^2 = 35.51$, $p < 0.001$. Genotypes: *20xUAS-IVS-CsChrimson::mVenus/+; R72F11-Gal4.AD/+; R38H09-Gal4.DBD/+* (black); *20xUAS-IVS-CsChrimson::mVenus/+; R72F11-Gal4.AD/R54B01-Gal4.AD; R38H09-Gal4.DBD/R46E07-Gal4.DBD* (red). Genotypes in (B-D) are the same as mentioned here.

(B) Cumulative plot of rolling duration. Statistics: Mann-Whitney test, $p = 0.0034$, n = 206, 83.

(C) A violin plot of end of first rolling bout for each larva during stimulation. Statistics: Mann-Whitney test, $p = 0.0047$, n = 57, 38.

(D) A violin plot of start of first crawling bout for each larva during stimulation. Statistics: Mann-Whitney test, $p = 0.045$, n = 107, 38.

(E) Binned larval rolling probabilities during first 5 s of stimulation. Error bars, 95% confidence interval. n = 192, 213. Statistics: Chi-square test, $\chi^2 = 64.81$, $p < 0.001$. Genotypes: *20xUAS-IVS-CsChrimson::mVenus/+; R72F11-Gal4.AD/+; R57F07-Gal4.DBD/+* (black); *20xUAS-IVS-CsChrimson::mVenus/+; R72F11-Gal4.AD/R54B01-Gal4.AD; R57F07-Gal4.DBD/R46E07-Gal4.DBD* (red). Genotypes in (F-H) are the same as mentioned here.

(F) Cumulative plot of rolling duration. Statistics: Mann-Whitney test, $p = 0.032$, n = 231, 71.

(G) A violin plot of end of first rolling bout for each larva during stimulation. Statistics: Mann-Whitney test, $p = 0.0047$, n = 129, 61.

(H) A violin plot of start of first crawling bout for each larva during stimulation. Statistics: Mann-Whitney test, $p < 0.001$, n = 159, 71.

$^{**}p < 0.01$, $^{***}p < 0.001$.

Legends for Supplementary figures

Figure S1. SS04185 inhibits rolling

(A) Crawling probabilities of larvae with the activation of SS04185-expressing neurons. Error bars, 95% confidence interval. Genotypes: *20xUAS-IVS-CsChrimson::mVenus/+;;* (black); *20xUAS-IVS-CsChrimson::mVenus/+; R54B01-Gal4.AD/+; R46E07-Gal4.DBD/+* (blue). Genotypes in (B-D) are the same as shown here. n = 308, 172. Statistics: Chi-square test, χ^2 = 2.32, $p > 0.05$.

(B) Turning probabilities of larvae with activation of SS04185-expressing neurons. Error bars, 95% confidence interval. n = 308, 172. Statistics: Chi-square test, $\chi^2 = 1.77$, $p > 0.05$.

(C) Hunching probabilities of larvae with activation of SS04185-expressing neurons. Error bars, 95% confidence interval. n = 308, 172. Statistics: Chi-square test, $\chi^2 = 0.35$, $p > 0.05$.

(D) Stopping probabilities of larvae with activation of SS04185-expressing neurons. Error bars, 95% confidence interval. n = 308, 172. Statistics: Chi-square test, $\chi^2 = 3.97$, $p = 0.046$.

(E) A violin plot of total time spent rolling for each individual larva during stimulation. Statistics: Mann-Whitney test, $p < 0.001$, n = 225, 89.

(F) Time series of crawling probabilities of SS04185 and Basin coactivation larvae (green) and Basin activation only larvae (black). Shaded areas show 95% confidential intervals of the crawling probabilities. Dashed lines display the window of optogenetic stimulation. Genotypes: *20xUAS-IVS-CsChrimson::mVenus/+; +; R72F11-Gal4/+* (control); *20xUAS-IVS-CsChrimson::mVenus/+; R54B01-Gal4.AD/+; R46E07-Gal4.DBD/R72F11-Gal4* (SS04185). Genotypes in (G-H) are the same as mentioned here. n = 228, 124.

(G) A violin plot of interval between first roll and next crawl. Statistics: Mann-Whitney test, $p > 0.05$, n = 151, 74.

(H) Crawling probabilities of SS04185 and Basin coactivation larvae (green) and Basin activation only larvae (black). Error bars, 95% confidence interval. n = 228, 124. Statistics: Chi-square test, $\chi^2 = 28.36$, $p < 0.001$.

(I) A violin plot of crawling speed ratio of larvae with null, SS04185 neuron, Basin, SS04185 neuron and Basin activation (from left to right). Crawling speed ratio = crawling speed 5 to 10 s after stimulation onset / crawling speed 0 to 5 s before stimulation onset. Statistics: Kruskal-Wallis test: H = 144, $p < 0.001$; Bonferroni corrected Mann-Whitney test: $p > 0.05$ for two groups on the left and two groups on the right. n = 308, 172, 227, 124. Genotypes from left to

right: 1) *20xUAS-IVS-CsChrimson::mVenus/+;;* ; 2) *20xUAS-IVS-CsChrimson::mVenus/+; R54B01-Gal4.AD/+; R46E07-Gal4.DBD/+*; 3) *20xUAS-IVS-CsChrimson::mVenus/+;; R72F11-Gal4/+*; 4) *20xUAS-IVS-CsChrimson::mVenus/+; R54B01-Gal4.AD/+; R46E07-Gal4.DBD/R72F11-Gal4.*

$^{**}p < 0.01$, $^{***}p < 0.001$.

Figure S2. SS04185-DN inhibits rolling

(A) Morphology of SS04185 neurons with split Gal4 inhibition in mushroom body (MB). GFP, Green. Anterior, up; dorsal view; scale bar, 100 μm. Genotype: *20xUAS-IVS-CsChrimson::mVenus/+; R13F02-LexA,LexAop-KZip^{+}/R54B01-Gal4.AD; R72F11-Gal4/R46E07-Gal4.DBD.*

(B) Time series of rolling probabilities of larvae with split Gal4 inhibition in MB (black), SS04185 activation (dark red), and both SS04185 activation and split Gal4 inhibition in MB (red). Shaded areas show 95% confidential intervals of rolling probabilities. The red bar and dashed lines display the window of optogenetic stimulation. Genotypes: *20xUAS-IVS-CsChrimson::mVenus/+; R13F02-LexA,LexAop-KZip^{+}/+; R72F11-Gal4/+* (black); *20xUAS-IVS-CsChrimson::mVenus/+; R54B01-Gal4.AD/+; R46E07-Gal4.DBD/R72F11-Gal4* (dark red); *20xUAS-IVS-CsChrimson::mVenus/+; R13F02-LexA,LexAop-KZip^{+}/R54B01-Gal4.AD; R72F11-Gal4/R46E07-Gal4.DBD* (red). Genotypes in (C) are the same as mentioned here.

(C) A violin plot of total time spent rolling for each individual larva during stimulation. Statistics: Kruskal-Wallis test: H = 21.05, $p < 0.001$; Bonferroni-corrected Mann-Whitney test, $p > 0.05$ for the two groups with SS04185 expression; $p < 0.001$ for the comparison between the group without SS04185 expression and the two groups with SS04185 expression, n = 66, 17, 21 from left to right.

(D) Time series of rolling probabilities of larvae with Basin activation (black), or Basin and MB coactivation (red). The red bar and dashed lines display the window of optogenetic stimulation eliciting larval escape responses. Shaded areas show 95% confidential intervals of rolling probabilities. n = 150, 143. Genotype: *20xUAS-IVS-CsChrimson::mVenus/+; +; R72F11-Gal4/+* (control); *20xUAS-IVS-CsChrimson::mVenus/+;+; MB247-Gal4/R72F11-Gal4* (MB247). Genotypes in (E) are the same as mentioned here.

(E) Binned larval rolling probabilities during the first 5 s of stimulation in (D). Error bars, 95% confidence interval. n = 150, 143. Statistics: Chi-square test, $\chi^2 = 3.80$, $p > 0.05$.

(F) and (G) show immunostaining of SS04185-expressing neurons. SS04185, Green. Anterior, up; dorsal view; scale bar, 100 μm Genotype: *w+, hs(KDRT.stop)FLP/13xLexAop2-IVS-CsChrimson::tdTomato; R54B01-Gal4.AD/72F11-LexA; 20xUAS-FRT(stop)-CsChrimson::mVenus/R46E07-Gal4.DB.* Genotypes in (H-K) are the same as mentioned here. (F) has only SS04185-MB expression, and (G) has both SS04185-DN and SS04185-MB expression.

(H) Time series of rolling probabilities of larvae with SS04185-MB activation (black), or SS04185-MB and SS04185-DN coactivation (red). The red bar and dashed lines display the window of optogenetic stimulation eliciting larval escape responses. Shaded areas show 95% confidential intervals of rolling probabilities.

(I) A violin plot of total time spent rolling for each individual larva during stimulation. Statistics: Mann-Whitney test, $p < 0.001$, n = 99, 124.

(J) A violin plot of end of first rolling bout for each larva during stimulation. Statistics: Mann-Whitney test, $p < 0.001$, n = 99, 124.

$^{**}p < 0.01$, $^{***}p < 0.001$.

Figure S4-1. SeIN128 is downstream of Basin and A00c neurons

(A) Connectivity among Basin, A00c, and SeIN128. Each line represents synaptic connections from the pre-synaptic neurons (left) to the post-synaptic neurons (right). Line widths are proportional to the counts of the synapses.

(B) Peak $\Delta F/F_0$ increased with increasing irradiance in both SeIN128 and A00c neurons. The orange line corresponds with Figure 4B; yellow line corresponds with Figure 4C; and green line corresponds with Figure 4D.

Figure S4-2. Synapses from SeIN128 to Basin-2 are located near Basin-2 outputs

(A) Basin-2 morphology and cell body location reported in EM reconstruction dataset (A1, left hemi-segment). Dorsal view. Red lines, presynaptic sites; cyan lines, postsynaptic sites.

(B) A zoomed-in view of the square in (A).

(C) SeIN128 morphology and cell body location reported in EM reconstruction dataset (right). Dorsal view. Red lines, presynaptic sites; cyan lines, postsynaptic sites.

(D) A zoomed-in view of the square in (C).

(E) Connections between SeIN128 and Basin-2. Dorsal view. Red lines, presynaptic sites of SeIN128; cyan lines, postsynaptic sites of Basin-2; brown lines, presynaptic sites of Basin-2.

(F) Zoomed-in views of squares in (E).

(G) EM view of left top panel in (F). Green, SeIN128. Blue, Basin-2. White arrows show SeIN128 presynaptic sites adjacent to Basin-2. Yellow arrows are two presynaptic sites of Basin-2.

Figure S5. SeIN128 is GABAergic

(A) Immunostaining of SeIN128 cell body (green) and glutamatergic neuron (magenta). Genotype: *10xUAS-IVS-mry::GFP/+; R54B01-Gal4.AD/+; R46E07-Gal4.DBD/+*.

(B) Immunostaining of SeIN128 cell body (green) and cholinergic neuron (magenta). Genotype: *10xUAS- IVS-mry::GFP/+; R54B01-Gal4.AD/+; R46E07-Gal4.DBD/+*.

In (A)-(B), white triangles indicate locations of SeIN128 cell bodies. Anterior, up; dorsal view; scale bar, 10 μm.

Figure S6. SeIN128 inhibition enhances rolling

(A) Time series of rolling probabilities of larvae with Basin activation (black), or SS04185 inhibition and Basin activation (red). Larvae were incubated with heat to trigger the effect of shibire^{ts1}. The red bar and dashed lines display the window of optogenetic stimulation eliciting larval escape responses. Shaded areas show 95% confidential intervals of rolling probabilities. Genotypes: *13xLexAop2-IVS-CsChrimson::mVenus;R72F11-LexA/+; 20xUAS-TTS-Shibire/+* (black); *13xLexAop2-IVS-CsChrimson::mVenus; R72F11-LexA/R54B01-Gal4.AD; 20xUAS-TTS-Shibire/R46E07-Gal4.DBD* (red). Genotypes in (B-G) are the same as mentioned here.

(B) Binned larval rolling probabilities during first 5 s of stimulation in (A). Error bars, 95% confidence interval. n = 134, 143. Statistics: Chi-square test, $\chi^2 = 12.33$, $p < 0.001$.

(C) A violin plot of total time spent rolling for each individual larva during stimulation. Statistics: Mann-Whitney test, $p > 0.05$, n = 85, 115.

(D) Cumulative plot of rolling duration. Statistics: Mann-Whitney test, $p > 0.05$, n = 219, 352.

(E) A violin plot of start of first rolling bout for each larva during stimulation. Statistics: Mann-Whitney test, $p > 0.05$, n = 85, 115.

(F) A violin plot of end of first rolling bout for each larva during stimulation. Statistics: Mann-Whitney test, $p = 0.013$, n = 85, 115.

(G) A violin plot of start of first crawling bout for each larva during stimulation. Statistics: Mann-Whitney test, $p = 0.034$, n = 32, 22.

$^{**}p < 0.01$, $^{***}p < 0.001$.

Figure S7. SeIN128 sends feedback inhibition to Basins

(A) A violin plot of total time spent rolling for each individual larva with GABAR-RNAi in their Basin neurons during stimulation. Statistics: Kruskal-Wallis test: H = 112.43, $p < 0.001$; Bonferroni-corrected Mann-Whitney test, $p < 0.001$ for all RNAi groups, n = 271, 194, 154, 178, 174 from left to right.

(B) A violin plot of start of first rolling bout for each larva during stimulation. Statistics: Kruskal-Wallis test: H = 86.50, $p < 0.001$; Bonferroni-corrected Mann-Whitney test, $p < 0.001$ for GABA-B-R1^2, GABA-B-R2, and GABA-A-R groups, n = 271, 194, 154, 178, 174 from left to right.

(C) A violin plot of end of first rolling bout for each larva during stimulation. Statistics: Kruskal-Wallis test: H=35.99, $p < 0.001$; Bonferroni-corrected Mann-Whitney test, $p < 0.001$ for GABA-B-R2 and GABA-A-R groups, n = 271, 194, 154, 178, 174 from left to right.

(D) A violin plot of start of first crawling bout for each larva during stimulation. Statistics: Kruskal-Wallis test: H = 53.07, $p < 0.001$; Bonferroni-corrected Mann-Whitney test, $p < 0.001$ for GABA-B-R1^2 group, n = 89, 119, 139, 135, 137 from left to right.

(E) Calcium transients (mean ± s.e.m.) represented by $\Delta F/F_0$ are evoked in Basin axons by optogenetic activation of Basin neurons various intensities. N = 9. Genotype: *20xUAS-Syn21-opGCaMP6s,10XUAS-Syn21-CsChrimson88::tdTomato/+;CyO/+;TM6/R72F11-Gal4*.

(F) Calcium transients (mean ± s.e.m.) in Basin axons represented by $\Delta F/F_0$ are decreased by optogenetic activation of SeIN128 neurons at various intensities. N = 10. Genotype: *20xUAS-Syn21-opGCaMP6s,10XUAS-Syn21-CsChrimson88::tdTomato/+;CyO/R54B01-Gal4.AD;R72F11-Gal4/R46E07-Gal4.DBD*.

For (E) to (F), irradiances from left to right are 0.04, 0.1, 0.3, 0.5, and 1.4 μW/mm^2. For each irradiance, individual traces are shown with gray lines, whereas the average of individuals is shown in black. Shaded gray area denotes period of optogenetic activation (0 to 1 s).

1014 $^{**}p < 0.01$, $^{***}p < 0.001$.

1015

1016 **Figure S8. SeIN128 inhibits rolling elicited by both Basin-2 and Basin-4 activation.**

1017 (A) and (B) show ethograms of Basin-2 activation (A) and Basin-4 activation (B). Each row
1018 represents an individual larva. Pink, blue, green, orange, and purple lines represent bouts of
1019 rolling, turning, crawling, backward crawling, and hunching. The red bar and dashed lines denote
1020 the time window during the period of neural activation. Genotypes: *20xUAS-IVS-*
1021 *CsChrimson::mVenus/+; R72F11-Gal4.AD/+; R38H09-Gal4.DBD/+* (A); *20xUAS-IVS-*
1022 *CsChrimson::mVenus/+; R72F11-Gal4.AD/+; R57F07-Gal4.DBD/+* (B). Genotypes in (C) are
1023 the same as mentioned here.

1024 (C) Cumulative plot of rolling duration. Statistics: Mann-Whitney test, $p < 0.001$, n = 681, 141.

1025 (D) Time series of rolling probabilities of larvae with Basin-2 activation (black), or SS04185 and
1026 Basin-2 coactivation (red). The red bar and dashed lines display the window of optogenetic
1027 stimulation eliciting larval escape responses. Shaded areas show 95% confidential intervals of
1028 rolling probabilities. Genotypes: *20xUAS-IVS-CsChrimson::mVenus/+; R72F11-Gal4.AD/+;*
1029 *R38H09-Gal4.DBD/+* (black); *20xUAS-IVS-CsChrimson::mVenus/+; R72F11-*
1030 *Gal4.AD/R54B01-Gal4.AD; R38H09-Gal4.DBD/R46E07-Gal4.DBD* (red). Genotypes in (E) are
1031 the same as mentioned here.

1032 (E) A violin plot of start of first rolling bout for each larva during stimulation. Statistics: Mann-
1033 Whitney test, $p < 0.001$, n = 57, 38.

1034 (F) Time series of rolling probabilities of larvae with Basin-4 activation (black), or SS04185 and
1035 Basin-4 coactivation (red). The red bar and dashed lines display the window of optogenetic
1036 stimulation eliciting larval escape responses. Shaded areas show 95% confidential intervals of
1037 rolling probabilities. Genotypes: *20xUAS-IVS-CsChrimson::mVenus/+; R72F11-Gal4.AD/+;*
1038 *R57F07-Gal4.DBD/+* (black); *20xUAS-IVS-CsChrimson::mVenus/+; R72F11-Gal4.AD/R54B01-*
1039 *Gal4.AD; R57F07-Gal4.DBD/R46E07-Gal4.DBD* (red). Genotypes in (G) are the same as
1040 mentioned here.

1041 (G) A violin plot of start of first rolling bout for each larva during stimulation. Statistics: Mann-
1042 Whitney test, $p > 0.05$, n = 129, 61.

1043 $^{**}p < 0.01$, $^{***}p < 0.001$.

1044

References

Burgos, A., Honjo, K., Ohyama, T., Qian, C. S., Shin, G. J., Gohl, D. M., Silies, M., Tracey, W. D., Zlatic, M., Cardona, A., & Grueber, W. B. (2018). Nociceptive interneurons control modular motor pathways to promote escape behavior in Drosophila. *Elife*, *7*. https://doi.org/10.7554/eLife.26016

Burrell, B. D. (2017). Comparative biology of pain: What invertebrates can tell us about how nociception works. *J Neurophysiol*, *117*(4), 1461-1473. https://doi.org/10.1152/jn.00600.2016

Campagner, D., Vale, R., Tan, Y. L., Iordanidou, P., Pavon Arocas, O., Claudi, F., Stempel, A. V., Keshavarzi, S., Petersen, R. S., Margrie, T. W., & Branco, T. (2023). A cortico-collicular circuit for orienting to shelter during escape. *Nature*, *613*(7942), 111-119. https://doi.org/10.1038/s41586-022-05553-9

Cattaert, D., & El Manira, A. (1999). Shunting versus inactivation: analysis of presynaptic inhibitory mechanisms in primary afferents of the crayfish. *J Neurosci*, *19*(14), 6079-6089. https://doi.org/10.1523/JNEUROSCI.19-14-06079.1999

Chalfie, M., & Sulston, J. (1981). Developmental genetics of the mechanosensory neurons of Caenorhabditis elegans. *Dev Biol*, *82*(2), 358-370. https://doi.org/10.1016/0012-1606(81)90459-0

Chalfie, M., Sulston, J. E., White, J. G., Southgate, E., Thomson, J. N., & Brenner, S. (1985). The neural circuit for touch sensitivity in Caenorhabditis elegans. *J Neurosci*, *5*(4), 956-964. https://doi.org/10.1523/JNEUROSCI.05-04-00956.1985

Chin, M. R., & Tracey, W. D., Jr. (2017). Nociceptive Circuits: Can't Escape Detection. *Curr Biol*, *27*(16), R796-R798. https://doi.org/10.1016/j.cub.2017.07.031

Dason, J. S., Cheung, A., Anreiter, I., Montemurri, V. A., Allen, A. M., & Sokolowski, M. B. (2020). Drosophila melanogaster foraging regulates a nociceptive-like escape behavior through a developmentally plastic sensory circuit. *Proc Natl Acad Sci U S A*, *117*(38), 23286-23291. https://doi.org/10.1073/pnas.1820840116

Dolan, M. J., Luan, H., Shropshire, W. C., Sutcliffe, B., Cocanougher, B., Scott, R. L., Frechter, S., Zlatic, M., Jefferis, G., & White, B. H. (2017). Facilitating Neuron-Specific Genetic Manipulations in Drosophila melanogaster Using a Split GAL4 Repressor. *Genetics*, *206*(2), 775-784. https://doi.org/10.1534/genetics.116.199687

Guo, D., & Hu, J. (2014). Spinal presynaptic inhibition in pain control. *Neuroscience*, *283*, 95-106. https://doi.org/10.1016/j.neuroscience.2014.09.032

Hu, C., Petersen, M., Hoyer, N., Spitzweck, B., Tenedini, F., Wang, D., Gruschka, A., Burchardt, L. S., Szpotowicz, E., Schweizer, M., Guntur, A. R., Yang, C. H., & Soba, P. (2017). Sensory integration and neuromodulatory feedback facilitate Drosophila mechanonociceptive behavior. *Nat Neurosci*, *20*(8), 1085-1095. https://doi.org/10.1038/nn.4580

Hu, Y., Wang, C., Yang, L., Pan, G., Liu, H., Yu, G., & Ye, B. (2020). A Neural Basis for Categorizing Sensory Stimuli to Enhance Decision Accuracy. *Curr Biol*, *30*(24), 4896-4909 e4896. https://doi.org/10.1016/j.cub.2020.09.045

Hwang, R. Y., Zhong, L., Xu, Y., Johnson, T., Zhang, F., Deisseroth, K., & Tracey, W. D. (2007). Nociceptive neurons protect Drosophila larvae from parasitoid wasps. *Curr Biol*, *17*(24), 2105-2116. https://doi.org/10.1016/j.cub.2007.11.029

Im, S. H., & Galko, M. J. (2012). Pokes, sunburn, and hot sauce: Drosophila as an emerging model for the biology of nociception. *Dev Dyn*, *241*(1), 16-26. https://doi.org/10.1002/dvdy.22737

Imambocus, B. N., Zhou, F., Formozov, A., Wittich, A., Tenedini, F. M., Hu, C., Sauter, K., Macarenhas Varela, E., Heredia, F., Casimiro, A. P., Macedo, A., Schlegel, P., Yang, C. H., Miguel-Aliaga, I., Wiegert, J. S., Pankratz, M. J., Gontijo, A. M., Cardona, A., & Soba, P. (2022). A neuropeptidergic circuit gates selective escape behavior of Drosophila larvae. *Curr Biol*, *32*(1), 149-163 e148. https://doi.org/10.1016/j.cub.2021.10.069

Isaacson, J. S., & Scanziani, M. (2011). How inhibition shapes cortical activity. *Neuron*, *72*(2), 231-243. https://doi.org/10.1016/j.neuron.2011.09.027

Kabra, M., Robie, A. A., Rivera-Alba, M., Branson, S., & Branson, K. (2013). JAABA: interactive machine learning for automatic annotation of animal behavior. *Nat Methods*, *10*(1), 64-67. https://doi.org/10.1038/nmeth.2281

Kaneko, T., Macara, A. M., Li, R., Hu, Y., Iwasaki, K., Dunnings, Z., Firestone, E., Horvatic, S., Guntur, A., Shafer, O. T., Yang, C. H., Zhou, J., & Ye, B. (2017). Serotonergic Modulation Enables Pathway-Specific Plasticity in a Developing Sensory Circuit in Drosophila. *Neuron*, *95*(3), 722. https://doi.org/10.1016/j.neuron.2017.07.023

1106 Kapfer, C., Glickfeld, L. L., Atallah, B. V., & Scanziani, M. (2007). Supralinear increase of
1107 recurrent inhibition during sparse activity in the somatosensory cortex. *Nat Neurosci*,
1108 *10*(6), 743-753. https://doi.org/10.1038/nn1909
1109 Manoim, J. E., Davidson, A. M., Weiss, S., Hige, T., & Parnas, M. (2022). Lateral axonal
1110 modulation is required for stimulus-specific olfactory conditioning in Drosophila. *Curr*
1111 *Biol*, *32*(20), 4438-4450 e4435. https://doi.org/10.1016/j.cub.2022.09.007
1112 Masson, J. B., Laurent, F., Cardona, A., Barre, C., Skatchkovsky, N., Zlatic, M., & Jovanic, T.
1113 (2020). Identifying neural substrates of competitive interactions and sequence transitions
1114 during mechanosensory responses in Drosophila. *PLoS Genet*, *16*(2), e1008589.
1115 https://doi.org/10.1371/journal.pgen.1008589
1116 McGann, J. P. (2013). Presynaptic inhibition of olfactory sensory neurons: new mechanisms and
1117 potential functions. *Chem Senses*, *38*(6), 459-474. https://doi.org/10.1093/chemse/bjt018
1118 Nakamizo-Dojo, M., Ishii, K., Yoshino, J., Tsuji, M., & Emoto, K. (2023). Descending
1119 GABAergic pathway links brain sugar-sensing to peripheral nociceptive gating in
1120 Drosophila. *Nat Commun*, *14*(1), 6515. https://doi.org/10.1038/s41467-023-42202-9
1121 Ohyama, T., Jovanic, T., Denisov, G., Dang, T. C., Hoffmann, D., Kerr, R. A., & Zlatic, M.
1122 (2013). High-throughput analysis of stimulus-evoked behaviors in Drosophila larva
1123 reveals multiple modality-specific escape strategies. *PLoS One*, *8*(8), e71706.
1124 https://doi.org/10.1371/journal.pone.0071706
1125 Ohyama, T., Schneider-Mizell, C. M., Fetter, R. D., Aleman, J. V., Franconville, R., Rivera-Alba,
1126 M., Mensh, B. D., Branson, K. M., Simpson, J. H., Truman, J. W., Cardona, A., & Zlatic,
1127 M. (2015). A multilevel multimodal circuit enhances action selection in Drosophila.
1128 *Nature*, *520*(7549), 633-639. https://doi.org/10.1038/nature14297
1129 Oikawa, I., Kondo, S., Hashimoto, K., Yoshida, A., Hamajima, M., Tanimoto, H., Furukubo-
1130 Tokunaga, K., & Honjo, K. (2023). A descending inhibitory mechanism of nociception
1131 mediated by an evolutionarily conserved neuropeptide system in Drosophila. *Elife*, *12*.
1132 https://doi.org/10.7554/eLife.85760
1133 Oleson, E. B., Beckert, M. V., Morra, J. T., Lansink, C. S., Cachope, R., Abdullah, R. A.,
1134 Loriaux, A. L., Schetters, D., Pattij, T., Roitman, M. F., Lichtman, A. H., & Cheer, J. F.
1135 (2012). Endocannabinoids shape accumbal encoding of cue-motivated behavior via CB1

receptor activation in the ventral tegmentum. *Neuron*, *73*(2), 360-373. https://doi.org/10.1016/j.neuron.2011.11.018

Onodera, K., Baba, S., Murakami, A., Uemura, T., & Usui, T. (2017). Small conductance Ca(2+)-activated K(+) channels induce the firing pause periods during the activation of Drosophila nociceptive neurons. *Elife*, *6*. https://doi.org/10.7554/eLife.29754

Palay, S. L. (1956). Synapses in the central nervous system. *J Biophys Biochem Cytol*, *2*(4 Suppl), 193-202. https://doi.org/10.1083/jcb.2.4.193

Pan-Vazquez, A., Wefelmeyer, W., Gonzalez Sabater, V., Neves, G., & Burrone, J. (2020). Activity-Dependent Plasticity of Axo-axonic Synapses at the Axon Initial Segment. *Neuron*, *106*(2), 265-276 e266. https://doi.org/10.1016/j.neuron.2020.01.037

Papadopoulou, M., Cassenaer, S., Nowotny, T., & Laurent, G. (2011). Normalization for sparse encoding of odors by a wide-field interneuron. *Science*, *332*(6030), 721-725. https://doi.org/10.1126/science.1201835

Peirs, C., & Seal, R. P. (2016). Neural circuits for pain: Recent advances and current views. *Science*, *354*(6312), 578-584. https://doi.org/10.1126/science.aaf8933

Pinault, D., Smith, Y., & Deschenes, M. (1997). Dendrodendritic and axoaxonic synapses in the thalamic reticular nucleus of the adult rat. *J Neurosci*, *17*(9), 3215-3233. https://doi.org/10.1523/JNEUROSCI.17-09-03215.1997

Ray, S., Aldworth, Z. N., & Stopfer, M. A. (2020). Feedback inhibition and its control in an insect olfactory circuit. *Elife*, *9*. https://doi.org/10.7554/eLife.53281

Schneider-Mizell, C. M., Bodor, A. L., Collman, F., Brittain, D., Bleckert, A., Dorkenwald, S., Turner, N. L., Macrina, T., Lee, K., Lu, R., Wu, J., Zhuang, J., Nandi, A., Hu, B., Buchanan, J., Takeno, M. M., Torres, R., Mahalingam, G., Bumbarger, D. J., . . . Costa, N. M. D. (2021). Structure and function of axo-axonic inhibition. *Elife*, *10*. https://doi.org/10.7554/eLife.73783

Stokes, C. C., & Isaacson, J. S. (2010). From dendrite to soma: dynamic routing of inhibition by complementary interneuron microcircuits in olfactory cortex. *Neuron*, *67*(3), 452-465. https://doi.org/10.1016/j.neuron.2010.06.029

Swierczek, N. A., Giles, A. C., Rankin, C. H., & Kerr, R. A. (2011). High-throughput behavioral analysis in C. elegans. *Nat Methods*, *8*(7), 592-598. https://doi.org/10.1038/nmeth.1625

1166 Takagi, S., Cocanougher, B. T., Niki, S., Miyamoto, D., Kohsaka, H., Kazama, H., Fetter, R. D.,
1167 Truman, J. W., Zlatic, M., Cardona, A., & Nose, A. (2017). Divergent Connectivity of
1168 Homologous Command-like Neurons Mediates Segment-Specific Touch Responses in
1169 Drosophila. *Neuron*, *96*(6), 1373-1387 e1376.
1170 https://doi.org/10.1016/j.neuron.2017.10.030
1171 Tracey, W. D., Jr., Wilson, R. I., Laurent, G., & Benzer, S. (2003). painless, a Drosophila gene
1172 essential for nociception. *Cell*, *113*(2), 261-273. https://doi.org/10.1016/s0092-
1173 8674(03)00272-1
1174 Veres, J. M., Fekete, Z., Muller, K., Andrasi, T., Rovira-Esteban, L., Barabas, B., Papp, O. I., &
1175 Hajos, N. (2023). Fear learning and aversive stimuli differentially change excitatory
1176 synaptic transmission in perisomatic inhibitory cells of the basal amygdala. *Front Cell*
1177 *Neurosci*, *17*, 1120338. https://doi.org/10.3389/fncel.2023.1120338
1178 Vogt, K., Aso, Y., Hige, T., Knapek, S., Ichinose, T., Friedrich, A. B., Turner, G. C., Rubin, G.
1179 M., & Tanimoto, H. (2016). Direct neural pathways convey distinct visual information to
1180 Drosophila mushroom bodies. *Elife*, *5*. https://doi.org/10.7554/eLife.14009
1181 Winding, M., Pedigo, B. D., Barnes, C. L., Patsolic, H. G., Park, Y., Kazimiers, T., Fushiki, A.,
1182 Andrade, I. V., Khandelwal, A., Valdes-Aleman, J., Li, F., Randel, N., Barsotti, E.,
1183 Correia, A., Fetter, R. D., Hartenstein, V., Priebe, C. E., Vogelstein, J. T., Cardona, A., &
1184 Zlatic, M. (2023). The connectome of an insect brain. *Science*, *379*(6636), eadd9330.
1185 https://doi.org/10.1126/science.add9330
1186 Yoshimura, Y., & Callaway, E. M. (2005). Fine-scale specificity of cortical networks depends on
1187 inhibitory cell type and connectivity. *Nat Neurosci*, *8*(11), 1552-1559.
1188 https://doi.org/10.1038/nn1565
1189 Yoshino, J., Morikawa, R. K., Hasegawa, E., & Emoto, K. (2017). Neural Circuitry that Evokes
1190 Escape Behavior upon Activation of Nociceptive Sensory Neurons in Drosophila Larvae.
1191 *Curr Biol*, *27*(16), 2499-2504 e2493. https://doi.org/10.1016/j.cub.2017.06.068
1192 Zheng, Z., Lauritzen, J. S., Perlman, E., Robinson, C. G., Nichols, M., Milkie, D., Torrens, O.,
1193 Price, J., Fisher, C. B., Sharifi, N., Calle-Schuler, S. A., Kmecova, L., Ali, I. J., Karsh, B.,
1194 Trautman, E. T., Bogovic, J. A., Hanslovsky, P., Jefferis, G., Kazhdan, M., . . . Bock, D.
1195 D. (2018). A Complete Electron Microscopy Volume of the Brain of Adult Drosophila
1196 melanogaster. *Cell*, *174*(3), 730-743 e722. https://doi.org/10.1016/j.cell.2018.06.019

1197

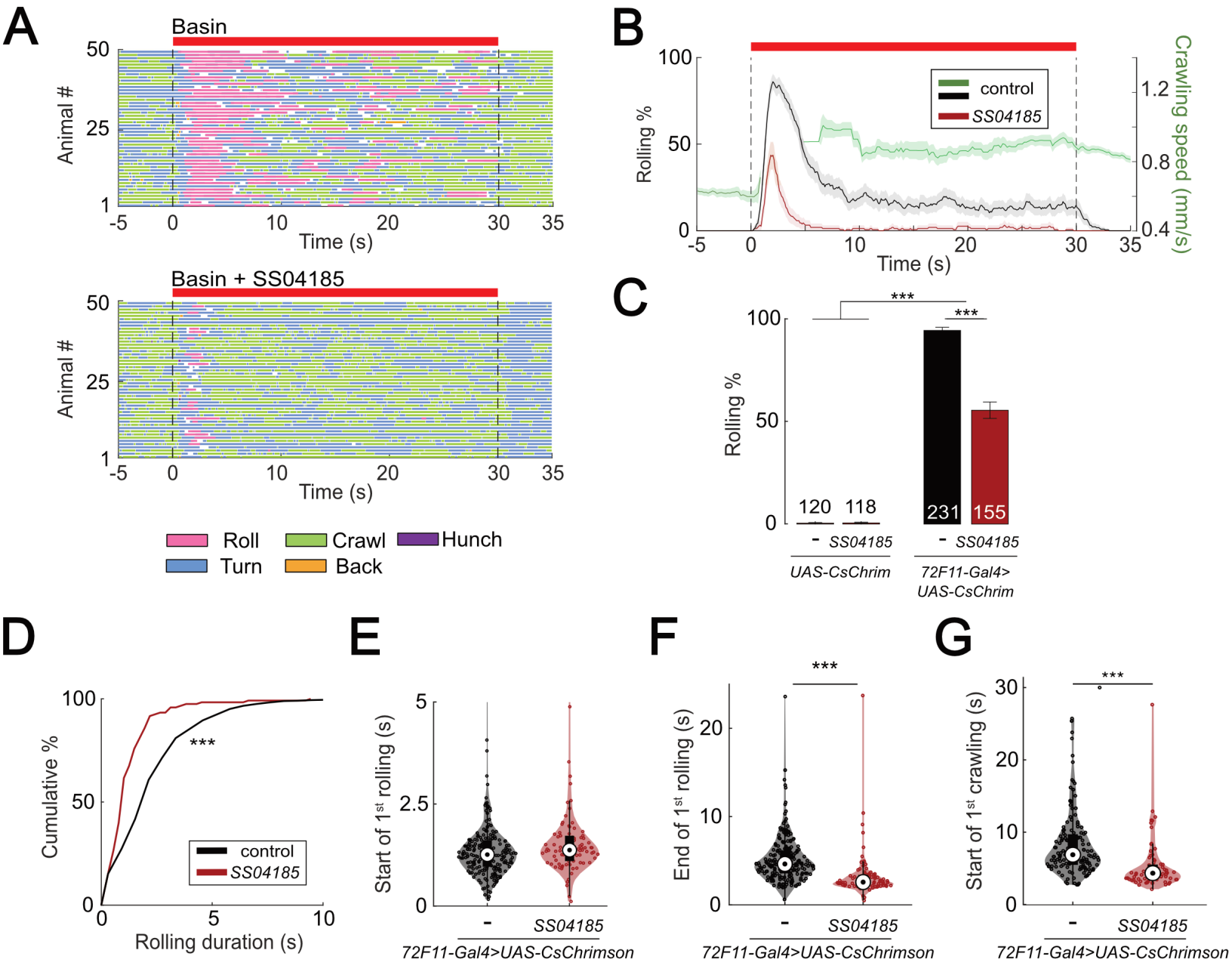

Figure 1. Activation of SS04185 inhibits rolling evoked by activation of Basin neurons

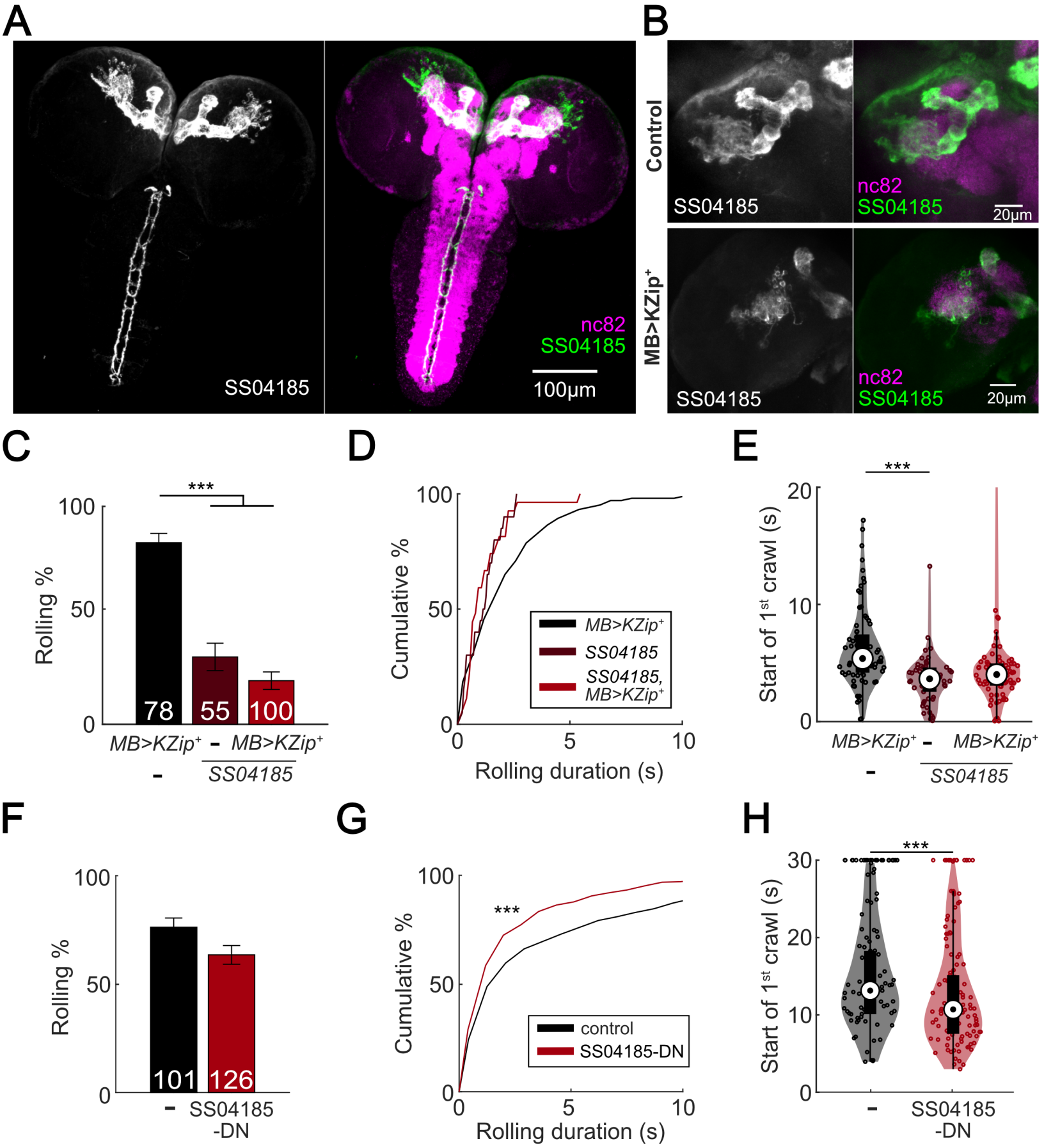

Figure2. SS04185-DN, but not SS04185-MB, inhibits rolling when co-activated with Basins

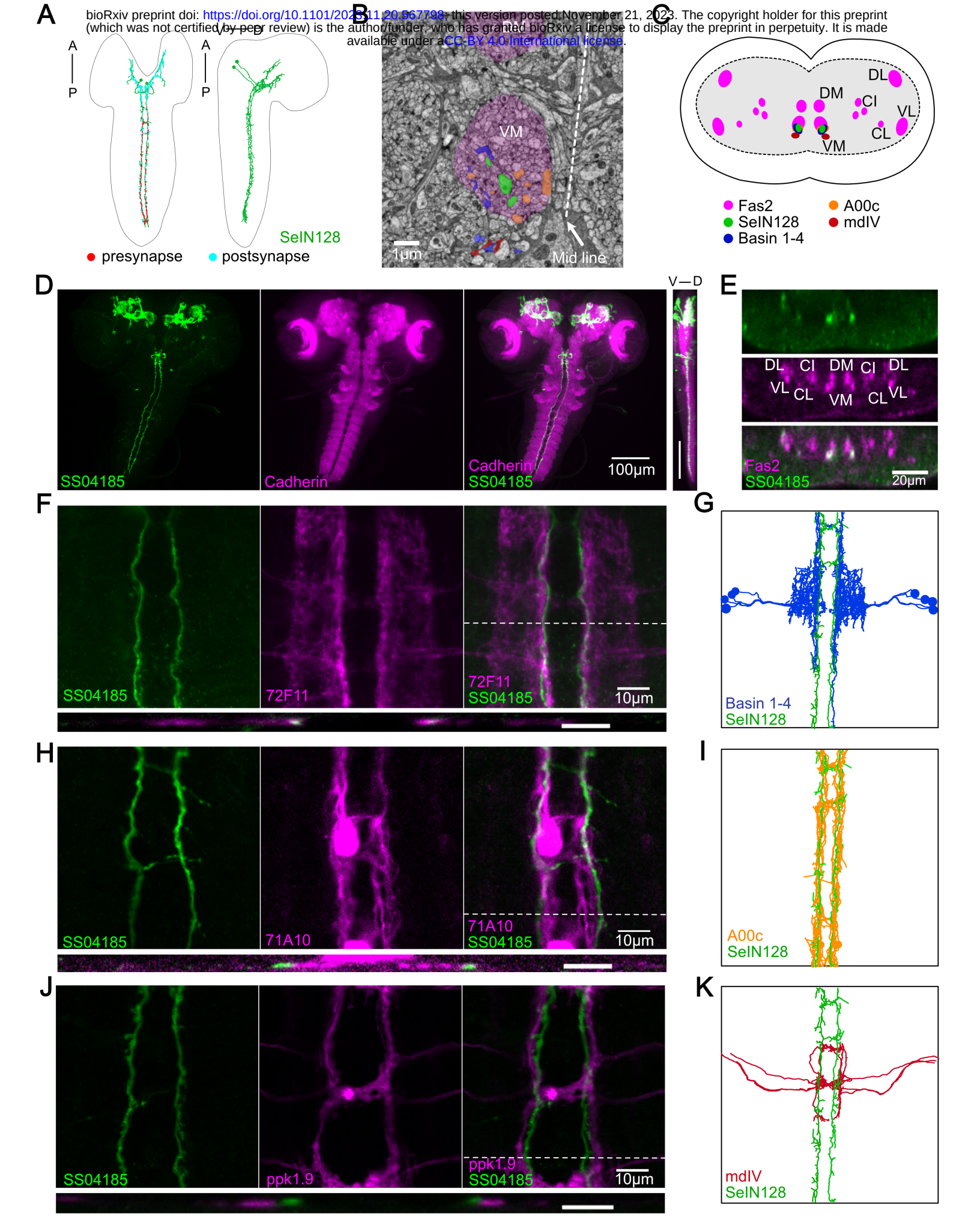

Figure 3. SS04185-DN is identical to SeIN128

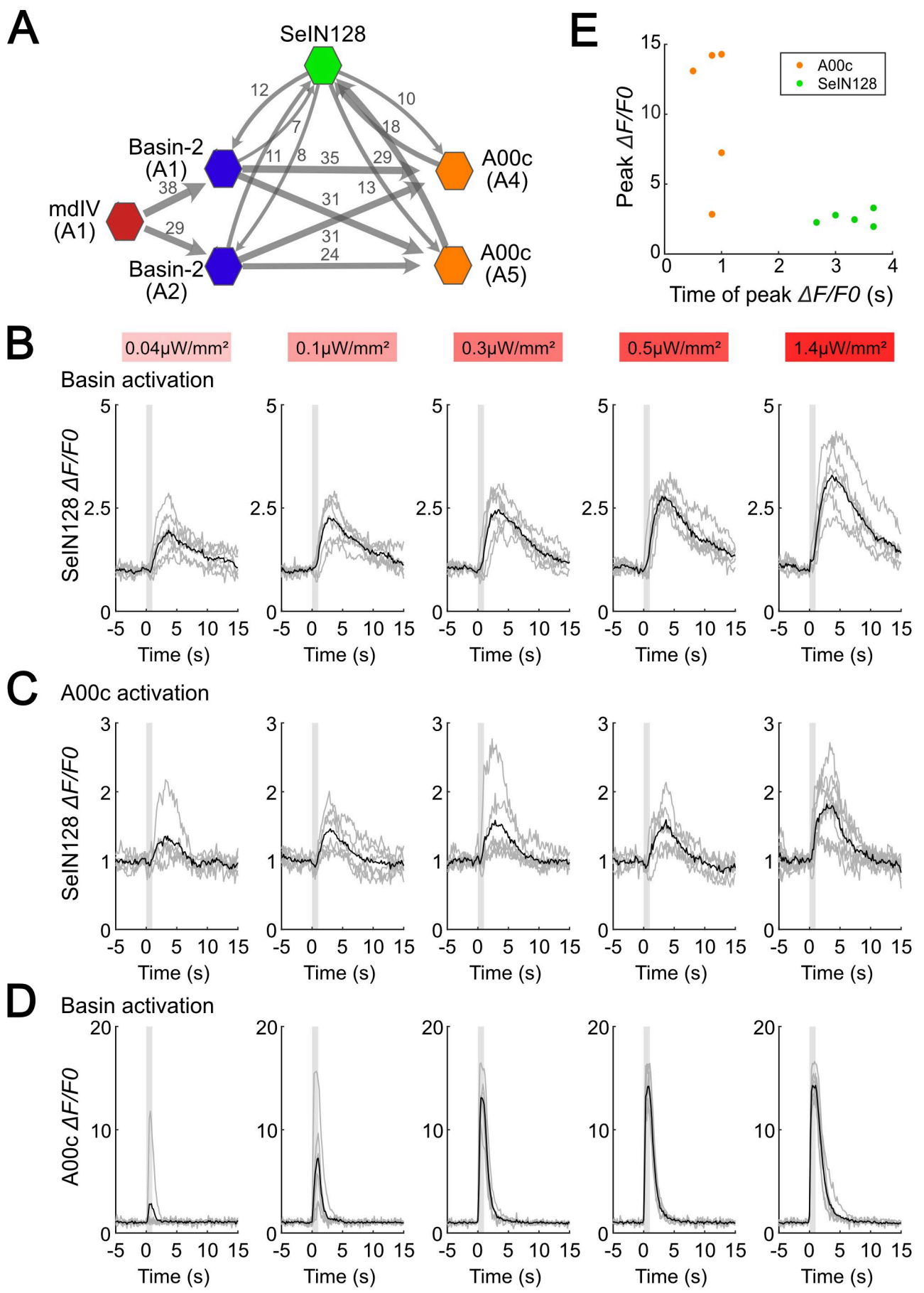

Figure 4. SeIN128 receives input from Basin and A00c neurons

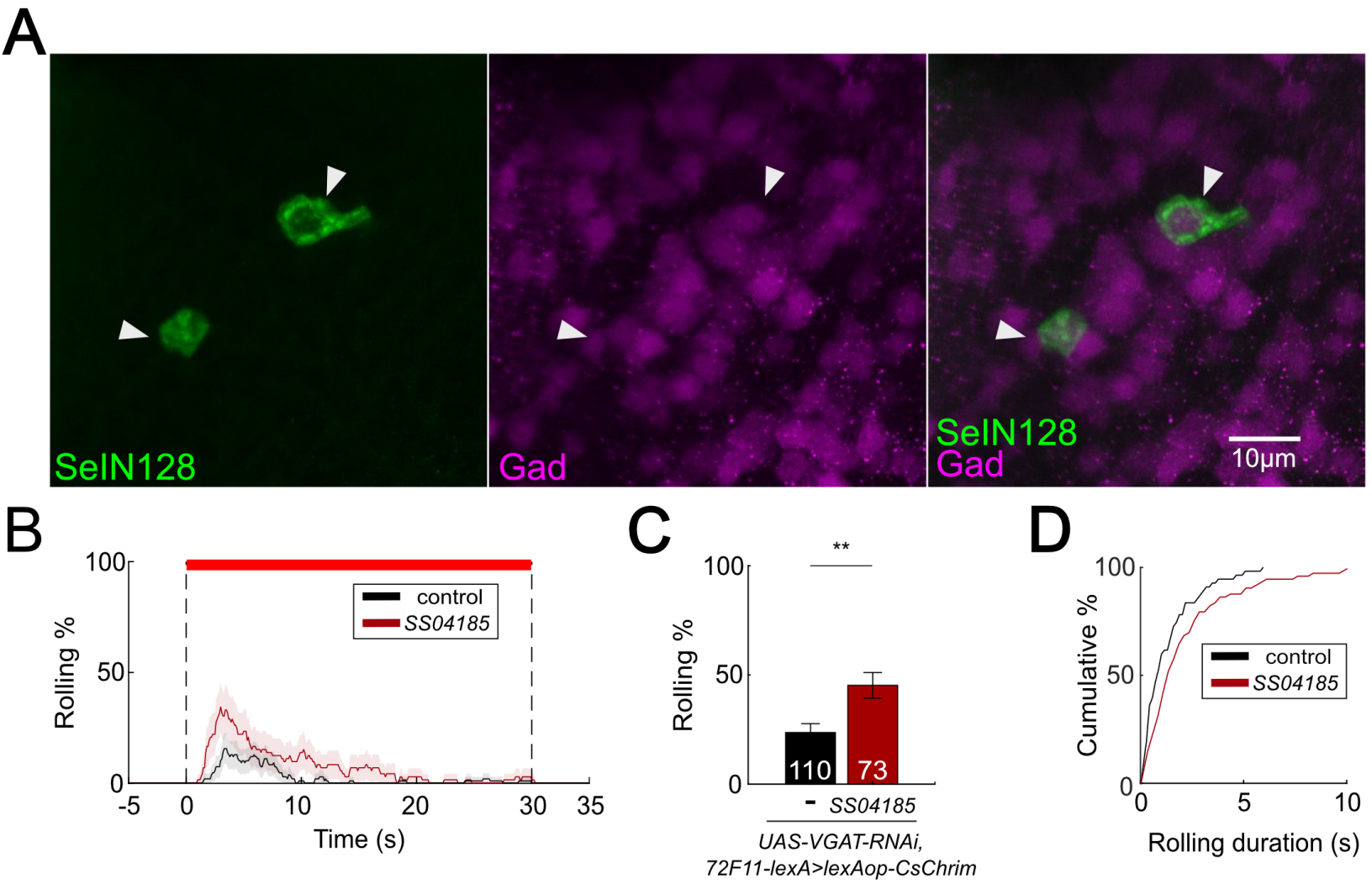

Figure 5. SeIN128 is GABAergic and negatively controls rolling

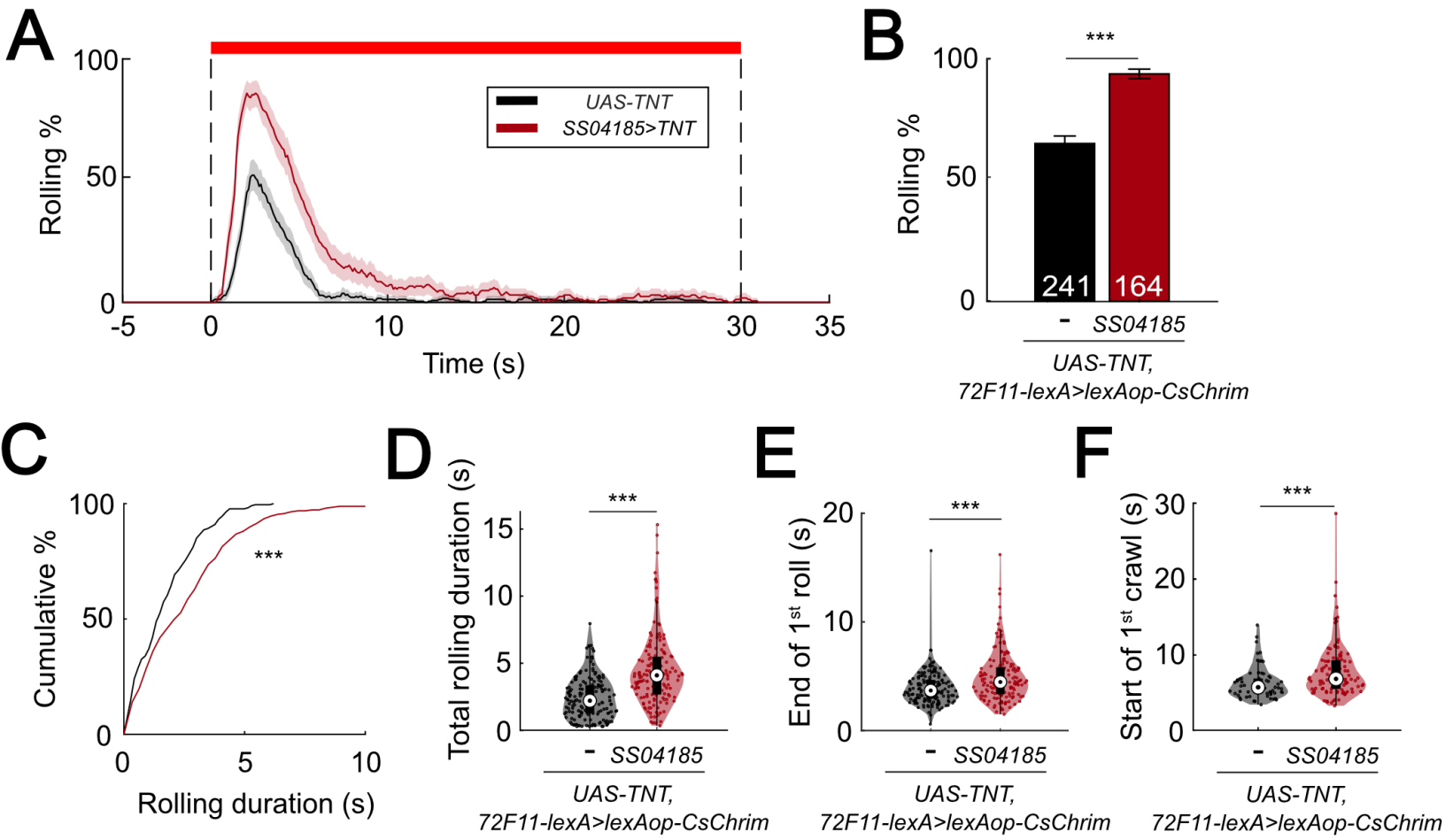

Figure 6. Inhibition of SeIN128 prolongs rolling and delays initiation of crawling

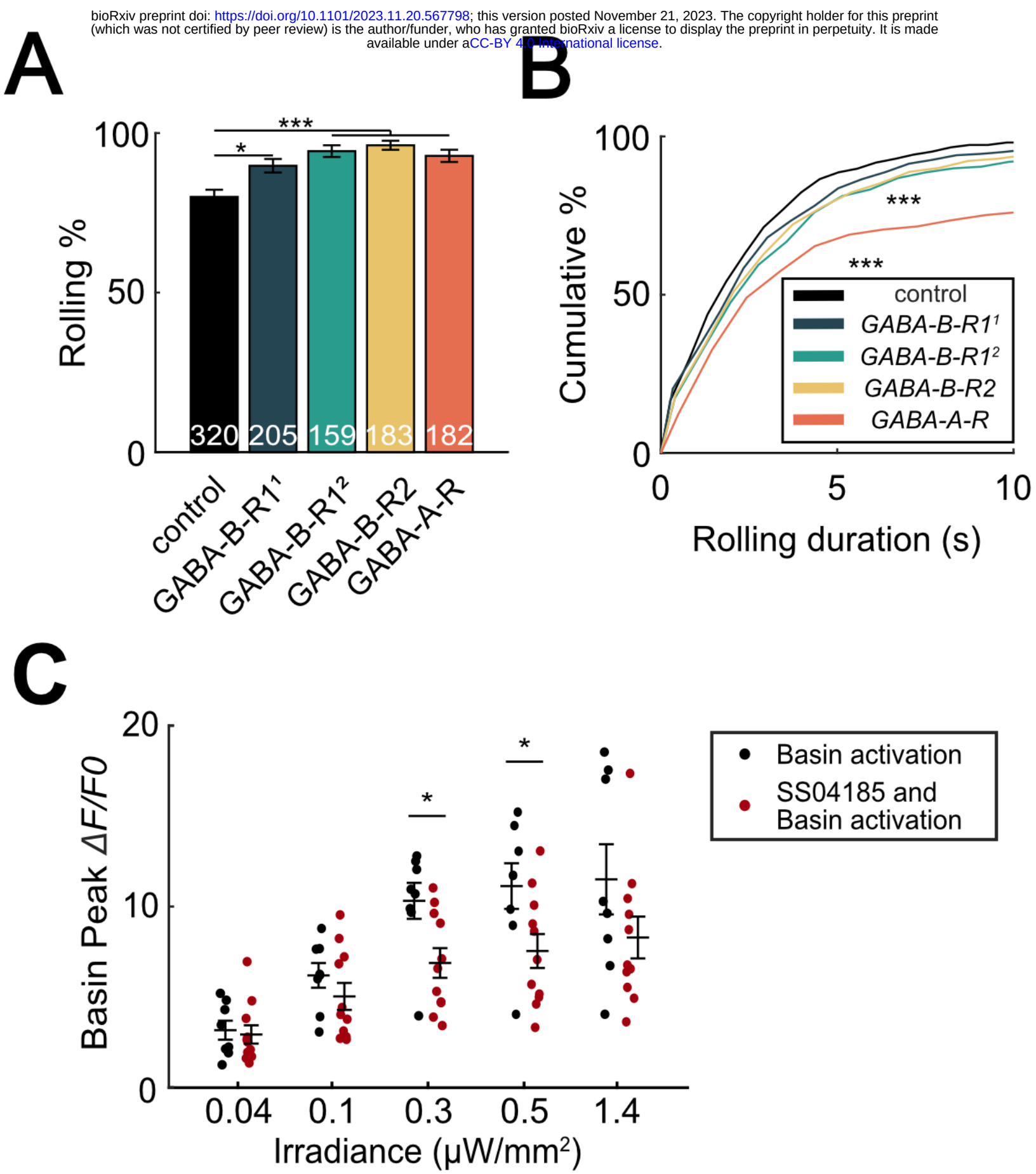

Figure7. SeIN128 sends feedback inhibition to Basins

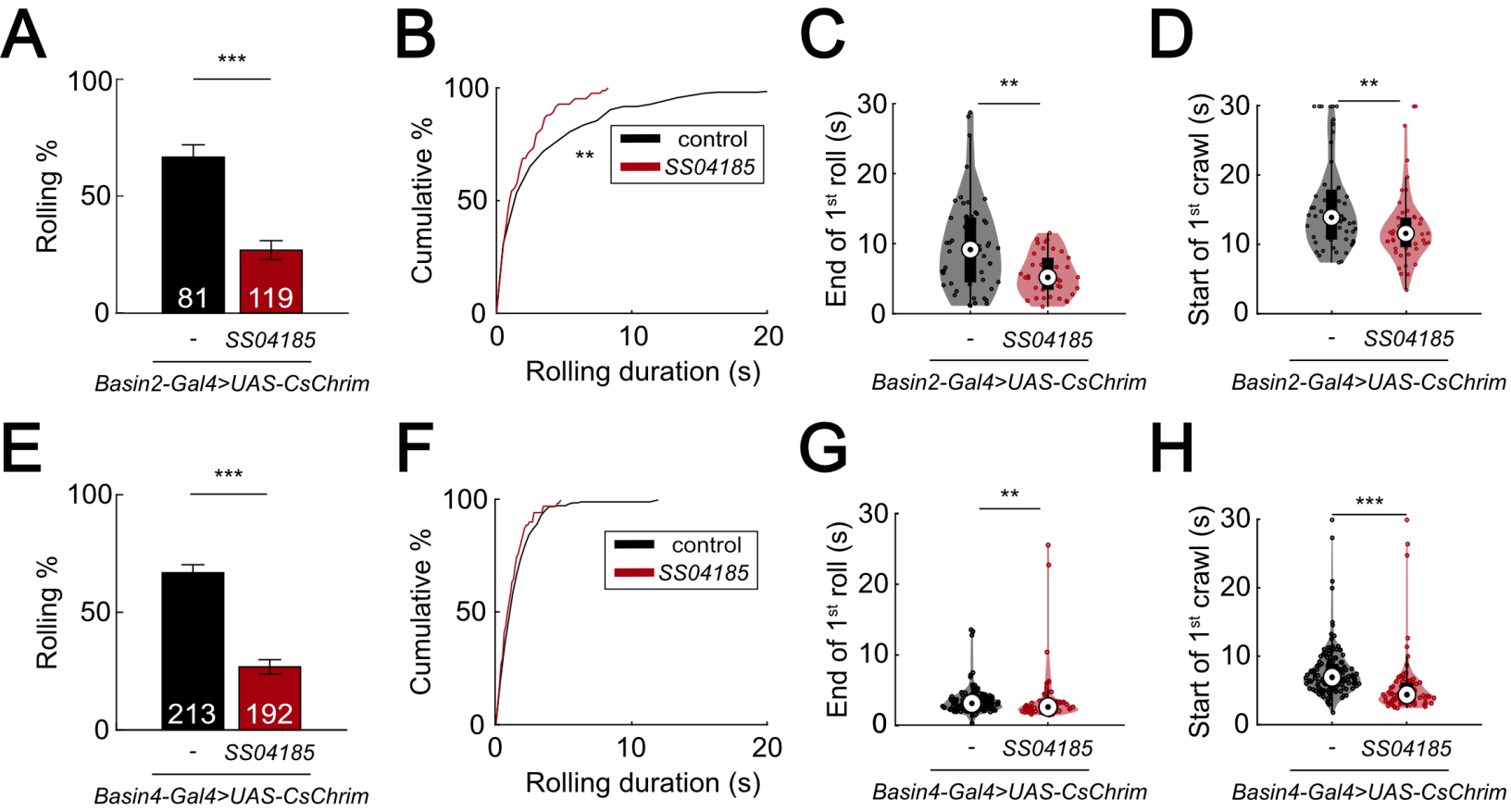

Figure 8. SeIN128 inhibits rolling elicited by both Basin-2 and Basin-4 activation